Stabilization of Expansive Soil using Rice Husk Biochar and Stimulation of Soil-Native Bacteria: Mechanical and Microstructural Analysis

Anas Bin Faruque , Shantanu Paul , Mohammad Shariful Islam

PII: S1226-7988(26)00117-0
DOI: https://doi.org/10.1016/j.kscej.2026.100620
Reference: KSCEJ 100620

To appear in: *KSCE Journal of Civil Engineering*

Received date: 1 December 2025
Revised date: 28 March 2026
Accepted date: 29 April 2026

Please cite this article as: Anas Bin Faruque , Shantanu Paul , Mohammad Shariful Islam , Stabilization of Expansive Soil using Rice Husk Biochar and Stimulation of Soil-Native Bacteria: Mechanical and Microstructural Analysis, *KSCE Journal of Civil Engineering* (2026), doi: https://doi.org/10.1016/j.kscej.2026.100620

Highlights:

- Combined MICP bio-stimulation and rice husk biochar (RHB) stabilizes expansive soils.
- Treatment reduces swell pressure by up to 93% and free swell strain by up to 85%.
- Significant strength increase: UCS by 106% and STS by 103% in stabilized soils.
- Calcite content boosts by 215%, pH rises to 8.95, confirming proper stabilization.
- Enhanced microbial activity, with urease-positive bacteria increasing significantly.

Stabilization of Expansive Soil using Rice Husk Biochar and Stimulation of Soil-Native Bacteria: Mechanical and Microstructural Analysis

Anas Bin Faruque[1] *(Corresponding Author)*

Lecturer

Email: anas@ce.buet.ac.bd

ORCiD: 0000-0003-4040-3173

Shantanu Paul[1]

Assistant Professor

Email: shantanu47@ce.buet.ac.bd

ORCiD: 0000-0002-3118-0513

Mohammad Shariful Islam[1]

Professor

Email: msharifulislam@ce.buet.ac.bd

ORCiD: 0000-0001-9620-2413

[1]Department of Civil Engineering

Bangladesh University of Engineering and Technology, Dhaka, Bangladesh

Abstract

This research explores the stabilization of expansive subgrade soils with microbially induced calcite precipitation (MICP) and rice husk biochar (RHB). The research focuses on addressing the shrink-swell behavior of expansive soils through bio-stimulation with indigenous ureolytic bacteria and the addition of RHB, which enhances biogeochemical reactions due to its pozzolanic properties and high cation exchange capacity. Various concentrations of RHB and MICP treatment durations were tested. Optimal results were achieved with 2% RHB and a four-day MICP mellowing period, significantly improving the soil's mechanical properties and reducing volume changes. The treatment decreased the free swell index by up to 98%, linear shrinkage by 85%, and swelling pressure by 93%, while increasing unconfined compressive strength and split tensile strength by over 100%. Enhancements were confirmed through SEM, FTIR analyses, and 16S metagenomic sequencing, demonstrating the efficacy of this dual-modality approach in enhancing stability and strength of expansive subgrade soil.

Keywords: MICP; Expansive Soil; Biochar; Stabilization; Shrink-Swell Behavior.

1. Introduction

Expansive soils show notable swelling and shrinkage due to varying moisture content. These soils exhibit swelling when they absorb water and shrinkage upon drying (Nelson and Miller, 1992; Seed et al., 1962). The instability caused by seasonal moisture changes generates internal stress within the soil, posing risks to structures built upon it. Light constructions are particularly vulnerable, experiencing problems such as building distortion, pavement heaving, slab fractures, and damage to water reservoirs and canal linings (Barman and Dash, 2022). This instability also impacts infrastructure such as irrigation systems, underground utilities, and railways, resulting in structural deformations. The recurring nature of these issues often results in maintenance expenses that surpass the initial construction costs (Chen, 1975; Ito, 2013). Buhler and Cerato (2007) observed that the annual damages from expansive subgrade soils in the USA could exceed $15 billion. Notably, the annual damage due to soil swelling often exceeds the combined yearly losses from other natural disasters (Jones and Holtz, 1973).

The main reason for volume instability in expansive subgrade soils is the presence of minerals like illite and montmorillonite. Montmorillonite is particularly influential due to its unique three-layer sheet structure and small crystallite size, which facilitate significant water absorption between layers. The weak van der Waals forces

between these layers allow for substantial volume changes with moisture variations, making montmorillonite a major factor in soil expansiveness (Das, 2019). Illite also contributes to soil swelling, albeit to a lesser extent than montmorillonite. This is due to its stronger ionic and hydrogen bonds, stabilized by potassium ions, which make its structure more rigid and limit its expansion and water absorption capacity (Das, 2019).

To overcome challenges in expansive soils, several stabilization methods are employed, such as compaction, chemical stabilization, pre-wetting, moisture barrier implementation, lime injection, and deep mixing, with selection depending on soil characteristics (Petry and Little, 2003; Zada et al., 2023; Ikeagwuani and Nwonu, 2019). While mechanical methods are widely used, they are often labor-intensive, time-consuming, and not always reliable, especially when dealing with pre-wetting cycles or problematic soils like expansive clays. Consequently, additional chemical stabilization is frequently required (Ikeagwuani and Nwonu, 2019). However, chemical stabilization, although common in road construction, presents environmental risks (Bu et al., 2018; Puppala and Pedarla, 2017; Ikeagwuani and Nwonu, 2019; Paul et al., 2024).

In response to growing environmental and health concerns associated with increasing industrial waste, utilization of industrial waste as sustainable substitutes to traditional chemical additives in soil stabilization has gained traction (Paul et al., 2023). Conventional disposal methods, primarily open dumping, are unsustainable and environmentally detrimental. The 2019 Global Waste Generation report projects a 70% increase in waste production by 2050, with the World Bank warning of a potential 3.4-billion-ton rise in waste generation, with 40% currently unmanaged (Vijayan and Parthiban, 2020; Ian Tiseo, 2023). Using industrial by-products as soil stabilizers reduces waste, lowers reliance on harmful materials, improves soil properties, and offers economic benefits (Sikder et al., 2026). Incorporating industrial by-products as alternative soil stabilizers offers a comprehensive solution by reducing waste generation, decreasing reliance on harmful stabilizers, enhancing soil properties, and providing economic benefits for waste management. Globally, the rice milling process yields a substantial by-product, rice husk, amounting to around 100 million tons annually (Alhassan and Mustapha 2007; Anupam et al. 2014). Producing biochar from rice husk through pyrolysis is very much cost-effective as the process is self-sufficient and environment friendly as it is a waste material (Villarreal and Wang, 2021).

Biochar is a porous, carbon-rich, fine solid produced through the thermochemical decomposition of biomass under limited oxygen conditions. Methods such as pyrolysis, carbonization, and hydrothermal processing are applied to produce biochar (Kong et al., 2014; Ren et al., 2014). Among these, pyrolysis is particularly suitable for large-scale biochar production. Biochar is typically produced from organic by-products from animal, agricultural, and

forestry wastes that undergo pyrolysis. In this process, biomass undergoes thermal decomposition under limited or no oxygen, yielding bio-oil, biochar, and syngas The relative yields of biochar, bio-oil, and syngas depend on processing conditions, and the reaction can be self-sustaining, as the combustion of syngas or part of the bio-oil and biochar supplies the required energy. From a theoretical standpoint, biochar is highly effective in treating expansive subgrade soils due to two primary factors: (1) biochar possesses a much greater capacity to absorb water compared to expansive clay minerals, allowing it to outperform in the competition for water, and (2) biochar treatment enhances soil permeability, hence decreasing the duration of water retention and consequently reducing the ultimate expansion deformation (Villarreal and Wang, 2021). Additionally, biochar's high porosity aids in the retention of nutrients and agrochemicals, benefiting plant growth (Inyang and Dickenson, 2015).

Existing research on improving soil characteristics using biochar mainly focuses on deformation, strength, and swell-shrink behavior. For instance, Zong et al. (2014) evaluated the effects of different types of biochar on clay settlement, strength, and surface cracking. Lu et al. (2014) explored how different rice husk biochar mixing percentages influenced the pore structure, swell-shrink behavior, and tensile strength. Likewise, Man et al. (2020) assessed the swell-shrink behavior of soil at varying biochar mixing percentages and grain sizes using a centrifuge. Sun et al. (2014) demonstrated that biochar can improve soil mass stability. Most previous studies on biochar-treated expansive soil have been conducted on loose soils, typical in agricultural settings, contrasting with the highly compacted soils used in engineered landfill and slope covers (Reddy et al., 2015; Ng et al., 2020; Garg et al., 2019). Villarreal and Wang (2021) conducted a feasibility study on the use of biochar to treat expansive soils, experimenting with three varying biochar percentages by weight (2%, 4%, and 6%). Their findings concluded that while the addition of biochar did not alter the liquid limit of the soil, it increased the plastic limit. Furthermore, biochar effectively restricted the expansion deformation of expansive soils, with an optimal biochar content identified at 2%. Pan et al. (2021) investigated the shrink-swell suppression mechanism of treated expansive soils with biochar derived from woodchips and pig manure. Their findings demonstrated that, for a given biochar type, the shrink-swell behavior of the modified soil samples dramatically decreased as the biochar content increased. X-ray diffraction (XRD) tests revealed that the water reactivity of the expansive soil was markedly decreased due to the compression of the hydrophilic mineral lattice. Additionally, the study showed that plant-based biochar significantly outperformed animal-based biochar in reducing swelling.

Microbially induced calcite precipitation (MICP) is gaining recognition as a sustainable method for enhancing the mechanical properties of porous materials. This innovative technique utilizes soil bacteria to precipitate calcium carbonate in situ through the process of ureolysis (Dejong et al. 2013; Tiwari et al. 2021). MICP has wide-ranging

applications in civil engineering, including the stabilization of retaining walls, embankments, and dams, erosion control, stabilization of sandy soils, improvement of foundation load-bearing capacities, and mitigation of soil liquefaction risks (Kavazanjian and Karatas 2008). Microorganisms play a crucial role in natural soil cementation by depositing binding agents within the soil voids (Ivanov and Chu, 2008). These microbes can induce the formation of various binding materials, including carbonates, silicates, phosphates, sulfides, and hydroxides of elements like calcium, magnesium, iron, manganese, and aluminum (DeJong et al., 2006). The effectiveness of microbial mineral precipitation is largely determined by the microbes' capacity to generate a high-pH environment via their metabolic activities (Douglas and Beveridge, 2006). The most prevalent form of microbial mineral precipitation in natural settings is calcium carbonate precipitation, which is driven by microbes producing the urease enzyme. This enzyme catalyzes the hydrolysis of urea, leading to the production of carbonic acid and ammonia (DeJong et al., 2006; Paul et al., 2026b; Paul et al., 2026a). The ammonia subsequently converts into ammonium ions, increasing the system's alkalinity. Carbonic acid transforms into bicarbonate, which then reacts with hydroxide ions to produce carbonate ions. When a calcium source is introduced into the system, Ca^{2+} ions combine with carbonate ions to form calcite.

MICP serves as a bridging agent between adjacent soil grains, improving shear strength and rigidity while decreasing permeability (Cheng and Cord-Ruwisch, 2014). The efficiency of MICP is influenced by multiple factors, such as calcium ion and dissolved inorganic carbon concentrations, pH, and the availability of nucleation sites (Hammes and Verstraete, 2002).

The practical application of MICP involves two primary strategies: bio-augmentation and bio-stimulation. Bio-augmentation introduces external bacteria into the soil to induce calcite precipitation but faces challenges such as bacterial survival, uneven distribution, long permeation times, high cultivation costs, and mixing precautions (DeJong et al., 2010; Tsesarsky et al., 2018). In contrast, bio-stimulation activates indigenous bacteria to precipitate calcium carbonate, offering advantages in resilience and spatial consistency, thus making it a more efficient and natural method for calcium carbonate precipitation in difficult terrains (Gomez et al., 2018).

Gomez et al. (2017) compared the efficacy of bio-augmentation using *Sporosarcina pasteurii* with bio-stimulation in sand, finding that bio-stimulation could achieve comparable bio-cementation improvements on a larger scale. Chittoori and Neupane (2019) evaluated both bio-augmentation and bio-stimulation for stabilizing two naturally expansive soils with varying plasticity, finding reduced soil plasticity and swelling characteristics, along with increased UCS. Additionally, Chittoori et al. (2020) observed that the pH of expansive soil rose from 8.3 to 9.7

within seven days after adding a bio-enrichment solution. This increase in pH coincided with a rise in calcite content from 3% to 8% and a significant reduction in the free swell index from 114% to 29%. pH values of 9.0 or higher indicate active urea hydrolysis, making them effective indicators for monitoring ureolysis and the activation of indigenous ureolytic microorganisms (Gomez et al., 2017). In a study by Islam et al. (2020) on MICP via bio-stimulation in clays, increased liquid limit (LL) and plastic limit (PL), improved unconfined compressive strength (UCS), reduced swelling, and a direct correlation between calcite precipitation and clay content were reported. Wang et al. (2023) observed in their study on bio-stimulated calcareous sand a decrease in compressibility as cementation content increased.

Previous studies also highlight that the effectiveness of MICP treatment is strongly dependent on the duration of the bio-stimulation or mellowing period, as it governs microbial activity, urea hydrolysis, and subsequent calcite precipitation. Tiwari et al. (2021) reported that a four-day treatment period resulted in significant strength improvement in expansive soils due to enhanced calcite formation. Similarly, Paul and Islam (2025) observed that soil strength increased progressively with mellowing duration up to four days, beyond which (six days) the improvement diminished, indicating the existence of an optimum treatment period. This behaviour is attributed to the balance between microbial activity and environmental conditions, where prolonged durations may reduce efficiency due to nutrient depletion or changes in soil chemistry. These findings suggest that short-term durations (e.g., 2 days) represent the early stage of microbial activation and calcite nucleation, while intermediate durations (e.g., 4 days) correspond to optimal bio-cementation conditions.

The long-term stability of MICP-induced cementation has been widely studied, with evidence indicating that biogenic calcite is generally stable but may undergo dissolution under adverse environmental conditions such as pH reduction or chemical exposure (Gat et al., 2017). Such dissolution can weaken cementation bonds; however, studies also report that dissolved carbonate may reprecipitate within pore spaces, contributing to recrystallization and potential self-healing of the soil structure under cyclic conditions.

Biochar holds potential for enhancing soil enzymatic activity by nourishing the medium with high concentrations of organic carbon, phosphorus, and ammonium nitrogen, making it a valuable substance for catalyzing urea hydrolysis and bio-cementation in the field. When introduced to soil, biochar can increase levels of these elements, which play a vital role in driving soil enzymatic activity (Prendergast-Miller et al., 2011; Romdhane et al., 2019; Wang et al., 2015; Jang and Jia, 2020). Mechanistically, RHB enhances in-situ biogeochemical reactions through three distinct pathways: (1) it serves as a nutrient reservoir, supplying organic carbon and nitrogen that fuel

microbial metabolism and stimulate urease enzyme production, thereby accelerating urea hydrolysis and the subsequent generation of carbonate ions; (2) its highly porous microstructure and large specific surface area provide abundant nucleation sites for heterogeneous calcite precipitation, promoting more spatially distributed and effective cementation at inter-particle contacts; and (3) its high amorphous silica content (72.11% SiO_2) enables pozzolanic reactions with calcium ions, producing calcium silicate hydrate (C-S-H) gel as a parallel cementation mechanism that supplements the MICP-derived calcite binding. Consequently, biochar can enhance biogeochemical reactions and urease activity within the soil biota, potentially leading to greater calcite precipitation through urea hydrolysis (Wang et al., 2015). Additionally, the large specific surface area of biochar particles can hold biological treatment reagents and work as a source of organic carbon, further promoting bacterial growth (Bailey et al., 2011). Zhao et al. (2020) reported that activated carbon positively affects the efficacy of MICP, noting that bacterial fixation rates and calcite content increased with the increment of activated carbon. Behzadipour and Sadrekarimi (2021) examined the effect of biochar-assisted bio-stimulation on sand. Their results showed that biochar-assisted MICP, utilizing native ureolytic bacteria in sand, could efficiently precipitate calcite particles and enhance the shear strength of the sand. This method was proved to be nearly as effective as the more expensive bioaugmentation technique using exogenous bacteria. Xu et al. (2023) developed a biochar-bacteria (2B) partnership designed to leverage the nutritional and sorption capacities of biochar. This 2B system was evaluated for its effectiveness in immobilizing cadmium (Cd) and its impact on soil properties and functions.

MICP-based stabilization has been successfully applied to a wide range of soils, including sands, clays, and expansive soils, consistently improving strength and durability. The effectiveness of the method depends on soil characteristics such as mineralogy and pore structure, but the underlying biocementation mechanism remains similar. Moreover, the incorporation of biochar has been shown to enhance MICP efficiency by providing additional surface area and favorable conditions for microbial activity. These findings suggest that the combined MICP–biochar approach can be extended to other problematic soils, such as organic or collapsible soils, although soil-specific validation is required.

Despite these studies, three critical research gaps remain unaddressed. First, while biochar-assisted MICP has been investigated in granular soils such as sand (Behzadipour and Sadrekarimi, 2021), its application to fine-grained expansive subgrade soils, which present fundamentally different challenges related to low permeability, high clay content, and shrink-swell behavior, has not been explored. Additionally, not all biochars are identical; their physical and chemical properties vary significantly depending on the feed and the pyrolysis temperature

(Cantrell et al., 2012; Gaskin et al., 2008; Hossain et al., 2011; Kloss et al., 2012; Singh et al., 2010). Second, previous studies on biochar-treated expansive soil reported reductions in shrink-swell behavior but also observed significant strength losses, and no study has investigated whether MICP bio-stimulation can offset this strength penalty. Third, despite the central role of microbial activity in MICP, no prior study on expansive soil stabilization has employed 16S metagenomic sequencing to characterize the microbial community response to treatment, meaning that the biological basis for observed improvements has remained unverified. To address these gaps, this study aims to integrate rice husk biochar (RHB) with MICP bio-stimulation to stabilize expansive subgrade soils for pavement applications. The core objectives of this research are: (1) to determine the optimal RHB content and MICP mellowing period that maximize strength improvement while minimizing shrink-swell behavior of expansive subgrade soil, (2) to evaluate whether the incorporation of MICP bio-stimulation can offset the strength reduction caused by biochar addition alone, thereby resolving a key limitation of biochar-only treatments reported in the literature, and (3) to characterize the chemical, microstructural, and microbiological changes responsible for the observed improvements through 16S metagenomic sequencing, an analytical dimension absent from existing MICP studies on expansive soils.

Based on the existing literature, the following hypotheses guided the experimental design: (H1) the combination of RHB and MICP bio-stimulation will produce a synergistic effect, whereby the pozzolanic activity of RHB and calcite precipitation from biostimulation together yield greater strength gains and shrink-swell reduction than either treatment alone; (H2) increasing the mellowing period from 2 to 4 days will enhance bio-cementation by allowing more complete urea hydrolysis and calcite precipitation; and (H3) the nutrient-rich composition of RHB (organic carbon, phosphorus, ammonium nitrogen) will promote the growth and metabolic activity of indigenous urease-positive bacteria, as detectable through 16S metagenomic sequencing.

To test these hypotheses, this research comprehensively assesses swell-shrink behavior using 1D swell tests, free swell index, and linear shrinkage tests. Strength enhancements are evaluated through unconfined compressive strength (UCS), split tensile strength (STS), and California bearing ratio (CBR) tests. The effectiveness of the stabilization process is evaluated by measuring pH and calcite content. Beyond these macroscopic assessments, scanning electron microscopy (SEM) is employed to examine the densification of the soil matrix, the morphology of precipitated calcite crystals at inter-particle contacts, and the reduction of voids and fissures following treatment. Fourier-transform infrared spectroscopy (FTIR) is used to identify the formation of C-O bonds characteristic of calcium carbonate and Si-O bonds indicative of C-S-H gel, thereby providing direct chemical evidence of the dual cementation pathways (MICP-derived calcite and pozzolanic C-S-H). Finally, 16S

metagenomic sequencing is performed to quantify the shift in microbial community composition from the native Actinobacteria-dominated population toward urease-positive phyla thereby directly linking RHB addition to enhanced biostimulation efficacy and establishing the microbiological basis for the observed improvements. The research holds significant potential in construction and geotechnical engineering, aiming to improve the safety of lightly loaded infrastructures like buildings, roads, and embankments built on expansive subgrade soils.

2. Materials and methods

2.1. Soil

The expansive subgrade soil used in this study was sourced from *Char* Biswanath, Sirajdikhan, Munshiganj (23°48′37″ N, 90°24′45″ E). It was treated with a combination of biostimulated MICP and RHB. The particle size was assessed using sieve analysis and hydrometer test according to ASTM D6913 (2004) and ASTM D7928 (2017) standards, respectively, and the results are displayed in Figure 1. Specific gravity and Atterberg limits were measured following ASTM D854 (2000) and ASTM D4318 (2005) standards, respectively. The soil's shrink-swell potential was assessed through a 1D swell test, linear shrinkage, and a free swell index test, in line with ASTM D4546 (2021), BS 1377 (1990), and IS 2720 (Part 40) (1991) guidelines, respectively. These physical properties are detailed in Table 1. Additionally, the soil's compaction properties were assessed via a standard proctor compaction test in line with ASTM D698 (2007), with results displayed in Figure 2. Classified as fat clay (CH) under the Unified Soil Classification System (USCS) (ASTM D2487, 2013), the soil's chemical composition is outlined in Table 2. Additionally, the soil sample, after being finely ground, underwent X-ray diffraction (XRD) analysis with the Empyrean model by Malvern Panalytical. The resulting XRD pattern, shown in Figure 3, was analyzed with Panalytical's X'pert Highscore Plus software. The analysis revealed that the soil composition includes 46.5% illite, 27.7% montmorillonite, 13.9% chlorite, and 11.9% albite. The existence of expansive clay minerals in the sample suggests that the soil has expansive properties.

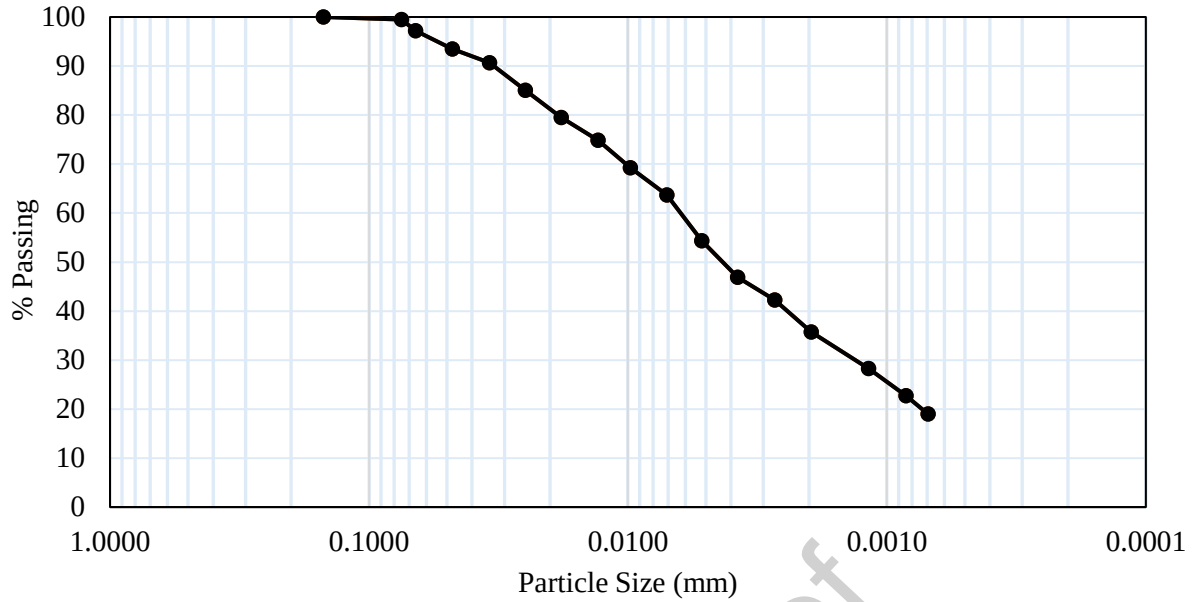

Figure 1. Particle size distribution curve of soil

Table 1. Physical properties of soil

Parameters	Value	Remarks
Specific Gravity	2.9	-
Sand (%)	0.5	-
Silt (%)	67.9	-
Clay (%)	31.6	-
Liquid Limit (%)	60	(50-70; High Degree of Expansion (IS: 1498, 1987))
Plastic Limit (%)	25	(>32; Very High Degree of Expansion (IS: 1498, 1987))
Plasticity Index (%)	35	(7-12; High Degree of Expansion (Holtz and Gibbs, 1956))
Shrinkage Limit (%)	10	(Medium Degree of Expansion (Asuri and Keshavamurthy, 2016))
Activity	0.90	-
Optimum Moisture Content (%)	24.96	-
Maximum Dry Density (kN/m^3)	15.09	-
Free Swell Strain (%)	54.4	(>30; Very High Degree of Expansion (Holtz and Gibbs, 1956))
Swell Pressure (kPa)	91	-
Free Swell Index (%)	81	(Medium Degree of Expansion (IS: 1498, 1987))
Linear Shrinkage (%)	16.2	-
USCS Soil Classification	Fat Clay (CH)	-

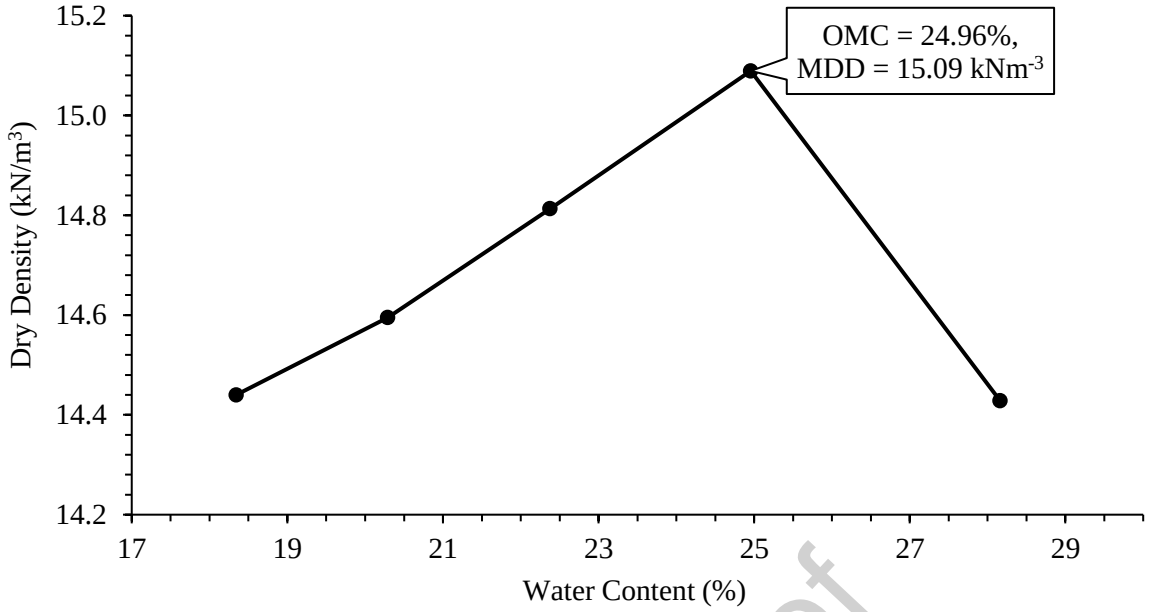

Figure 2. Compaction curve of soil from standard proctor compaction test

2.2. Treatment solutions

The biomineralization technique employed in this study involves the use of enrichment and cementation solutions, essential for the reliable formation of calcite within the soil mass. This method is crucial in creating an optimal habitat for the flourishing of native bacteria, which is indispensable for soil stabilization through MICP bio-stimulation.

Table 2. Chemical composition of soil by X-ray fluorescence (XRF) test

Compound	% by wt
SiO_2	60.14
Al_2O_3	14.44
Fe_2O_3	12.79
CaO	4.22
MgO	3.83
K_2O	1.83
TiO_2	1.47
Na_2O	0.59
P_2O_5	0.18
BaO	0.12
MnO	0.10
SO_3	0.10
Cr_2O_3	0.07
Loss on Ignition	0.12

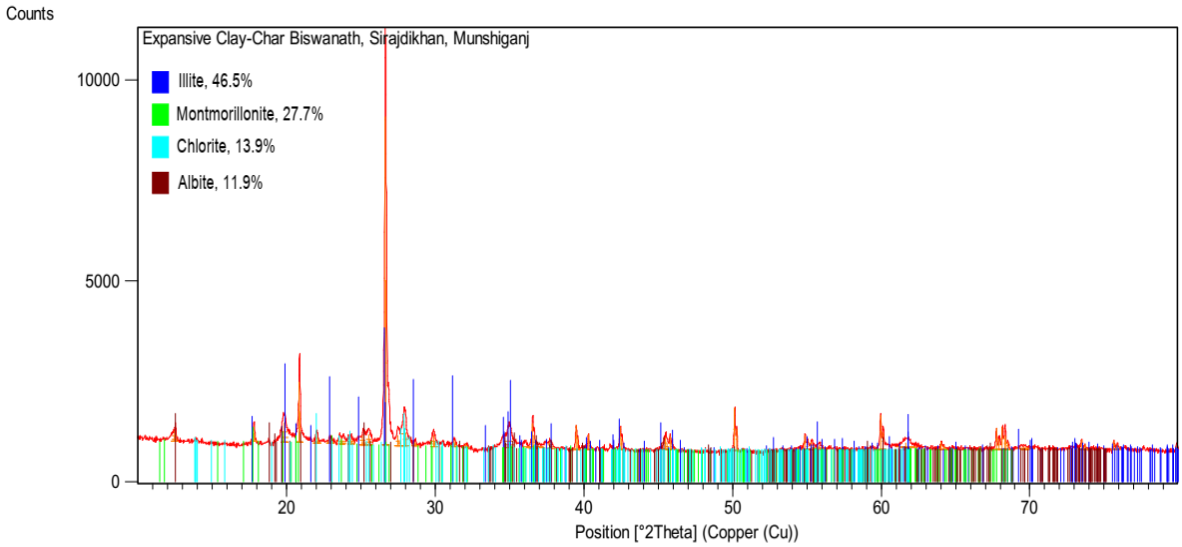

Figure 3. XRD analysis of the soil sample

Table 3 depicts the composition of the treatment solutions. The enrichment solution was explicitly formulated to foster gram-positive bacteria's growth, creating a supportive environment for bacterial proliferation. It comprised 100 mM sodium acetate ($C_2H_3NaO_2$), 333 mM urea (CH_4N_2O), and 2.0 g/L of nutrient broth, echoing the composition utilized by Tiwari et al. (2021). This blend of nitrogen, carbon, and essential nutrients mirrors other research, notably Gomez et al. (2017) and Chittoori et al. (2019), who also employed sodium acetate and urea, highlighting the efficacy of these components in stimulating bacterial activity. The use of 2.0 g/L nutrient broth aligns with the broader scientific consensus on its critical role in supplying minerals, vitamins, and amino acids essential for the sustenance of indigenous soil bacteria, as supported by Wang et al. (2023) and Tiwari et al. (2021).

The cementation solution study created conditions conducive to calcite precipitation by integrating 250 mM calcium chloride ($CaCl_2$) into the enrichment mix, in harmony with the results of Islam et al. (2020) and Chittoori et al. (2019). The composition of the treatment solutions used in this research balances enhancing microbial activity for calcite formation with the necessity of maintaining ecological equilibrium within the soil. Using distilled water as the base solvent further demonstrates the commitment to achieving a controlled and replicable experimental setup.

Table 3. Ingredients of the treatment solutions

Ingredients	Solution Type	
	Enrichment Solution	Cementation Solution
Nutrient Broth (g/L)	2	2
Urea (mM)	333	333
Sodium Acetate (mM)	100	100
Calcium Chloride (mM)	×	250

2.3. Rice husk biochar

The rice husk utilized in this research was sourced from an auto rice mill in Keraniganj, Dhaka. Outline of the preparation of RHB is depicted in the Figure 4 using a flow diagram. The pyrolysis process was conducted using a custom-made stainless-steel apparatus comprising a cylindrical drum, a cone, and a cylindrical duct. To initiate the process, the ignition cone was filled with flammable materials such as straw and wood. The filled cone was then inverted and placed inside the cylindrical drum, which was subsequently filled with rice husk. The material inside the cone was ignited, and the cylindrical duct was positioned over the inverted cone to facilitate the release of smoke at a higher elevation. Additional flammable material was supplied through the duct as needed.

The pyrolysis process lasted approximately four hours, during which the rice husk surrounding the inverted cone gradually transformed into biochar due to the high temperatures (approximately 350-600 °C) and the lack of oxygen near the ignition cone. The temperature was continuously monitored using an infrared temperature gun. The rice husk was periodically refilled and stirred throughout the process. After about four hours, the fire was extinguished with water, and the apparatus was covered with a plastic sheet and rope to suffocate the fire due to the absence of oxygen, allowing it to cool down gradually. Once the fire was completely extinguished, the rice husk biochar was carefully extracted from the drum and oven-dried for 24 hours. The dried biochar was then ground and sieved through a #200 (0.075 mm) sieve to make it suitable for use in expansive subgrade soil treatments. The setup involved in the RHB production process along with the major steps are depicted in Figure 5.

The chemical analysis of the RHB specimen reveals a high amorphous silicon dioxide (SiO_2) content of 72.11%, underscoring its pozzolanic potential (Table 4). The RHB used in this research had a specific gravity of 1.534.

The FTIR spectrum of RHB, shown in Figure 6, highlights the existence of various functional groups. Key absorption bands correspond to specific vibrational modes of the chemical bonds within the RHB. The prominent band at 1035.587 cm^{-1} is indicative of Si-O-Si asymmetric stretching vibrations, characteristic of the silicates in RHB (Kaleli et al., 2020; Panda et al., 2020). The 788.261 cm^{-1} region exhibits bands associated with O-Si-O

bending vibrations, suggesting a structured silica network (Kaleli et al., 2020; Singh et al., 2019). Additionally, the band at 3324.195 cm^{-1} corresponds to -OH bending vibrations, indicating hydroxyl groups, while the 1599.663 cm^{-1} band corresponds to -C=O, which may overlap with hydroxyl species in RHB (Hossain et al. 2020). The presence of smooth and distinct peaks within the RHB spectrum indicates its amorphous nature, a typical attribute of silica derived from agricultural residues like rice husks (Singh et al., 2019).

SEM analysis of rice husk biochar was conducted to perform the microstructural analysis, which is depicted in Figure 7. The SEM images reveal the surface morphology of the RHB, showcasing its highly porous structure. This porosity is crucial as it enhances the RHB's ability to absorb and retain nutrients and water, making it effective for soil treatment (Villarreal and Wang, 2021). The high surface area provided by these pores also facilitates microbial activity (Behzadipour and Sadrekarimi, 2021), which is beneficial for the MICP process by providing more nucleation sites for calcite precipitation. This, in turn, enhances the soil's mechanical properties and reduces its swell-shrink potential. The detailed microstructural characteristics observed through SEM highlight the potential of RHB as a sustainable amendment for enhancing soil properties in geotechnical engineering applications. Additionally, the EDX elemental analysis results in Figure 8 shows that RHB is primarily composed of carbon, oxygen, silicon, and nitrogen, echoing the findings of Jindo et al. (2014).

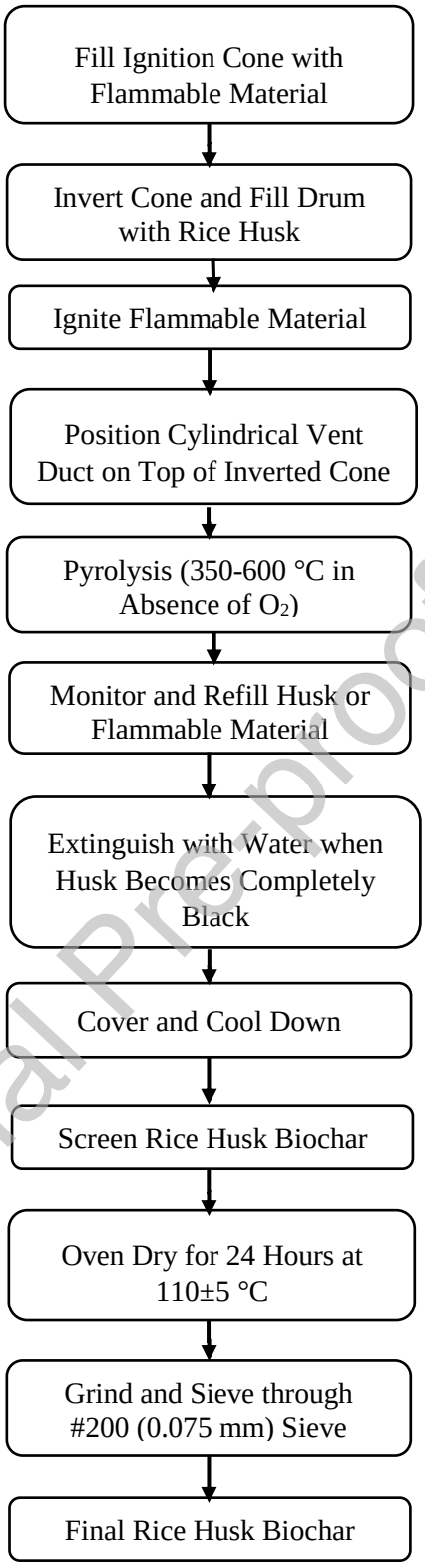

Figure 4. Outline of the preparation of rice husk biochar

(a) (b)

(c) (d)

Figure 5. Production of rice husk biochar- (a) Custom setup of apparatus used, (b) Initial rise in temperature measured with infrared temperature gun, (c) Maximum temperature inside the apparatus, and (d) Produced rice husk biochar

Table 4. Chemical composition of RHB by XRF test

Compound	% by wt
SiO_2	72.11
K_2O	9.49
CaO	6.72
P_2O_5	2.61
SO_3	2.00
MgO	1.61
Cl	1.55
Fe_2O_3	1.34
Al_2O_3	0.75
MnO	0.75
Bi_2O_3	0.37
TiO_2	0.29
Na_2O	0.22
ZnO	0.12
Rb_2O	0.06
ZrO_2	0.01

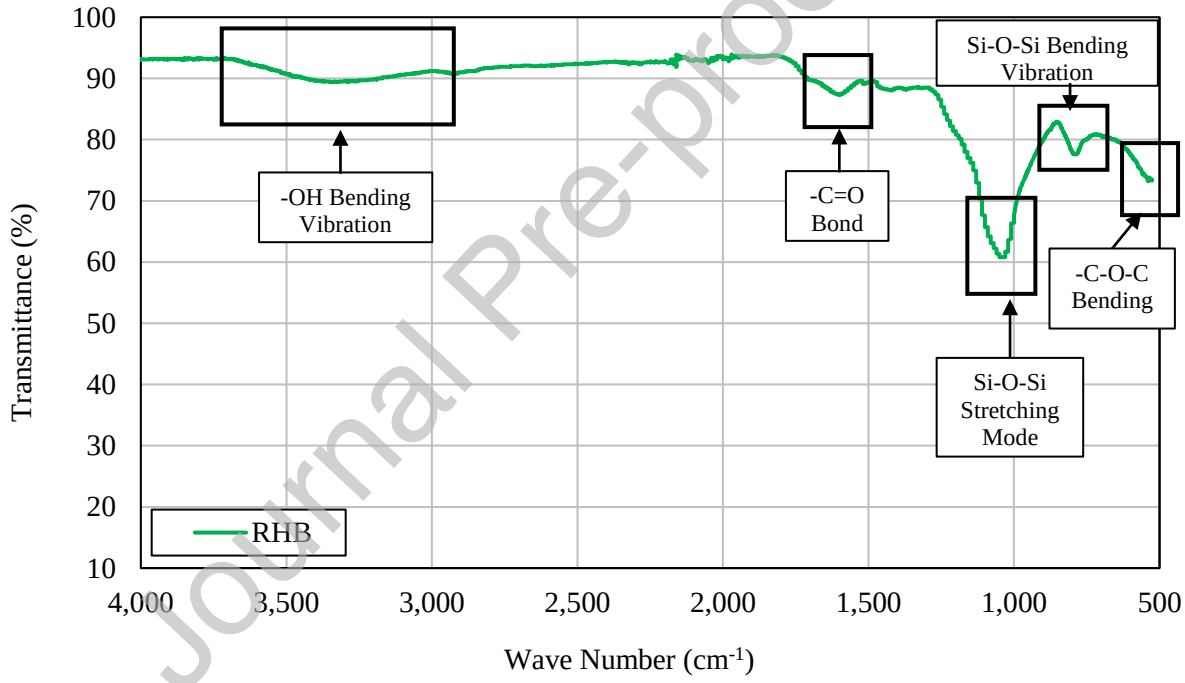

Figure 6. FTIR spectra of rice husk biochar

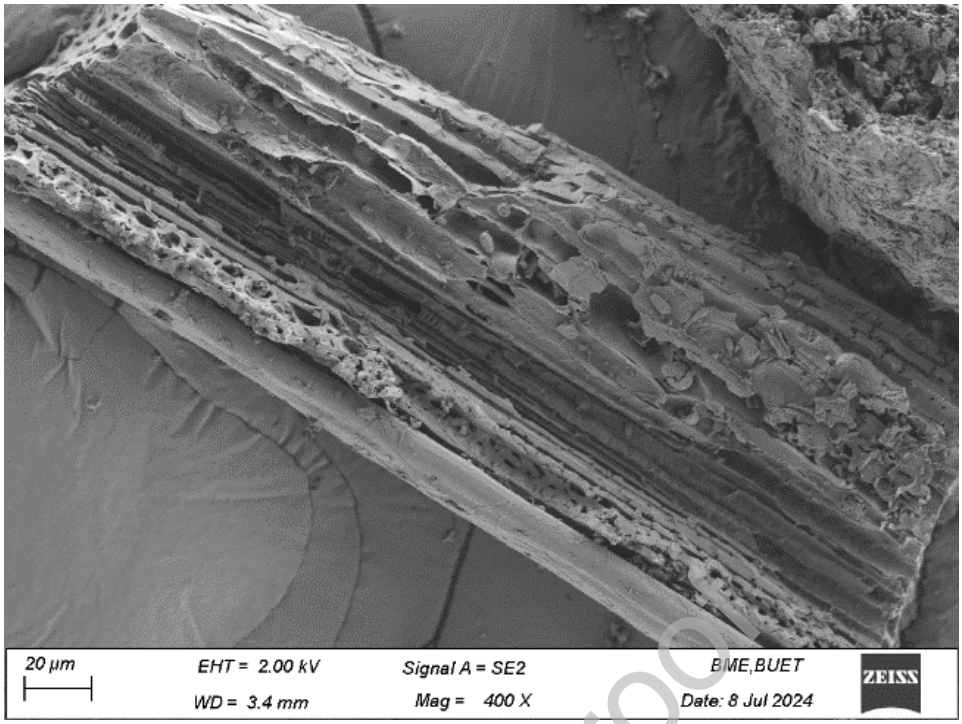

(a)

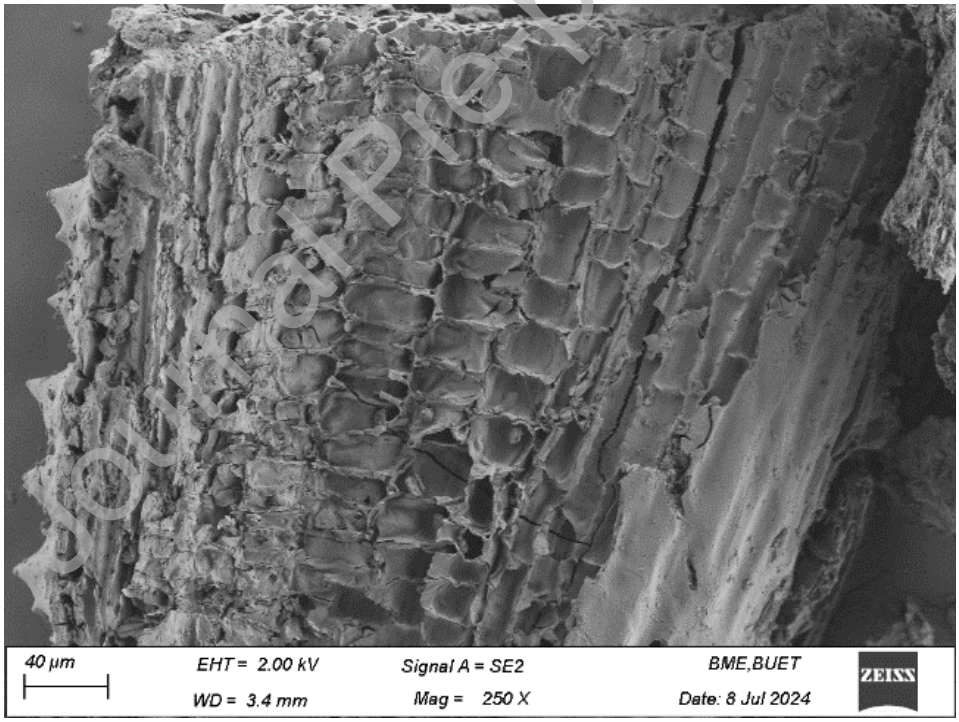

(b)

Figure 7. SEM images of RHB- (a) Whole particle, (b) Surface morphology

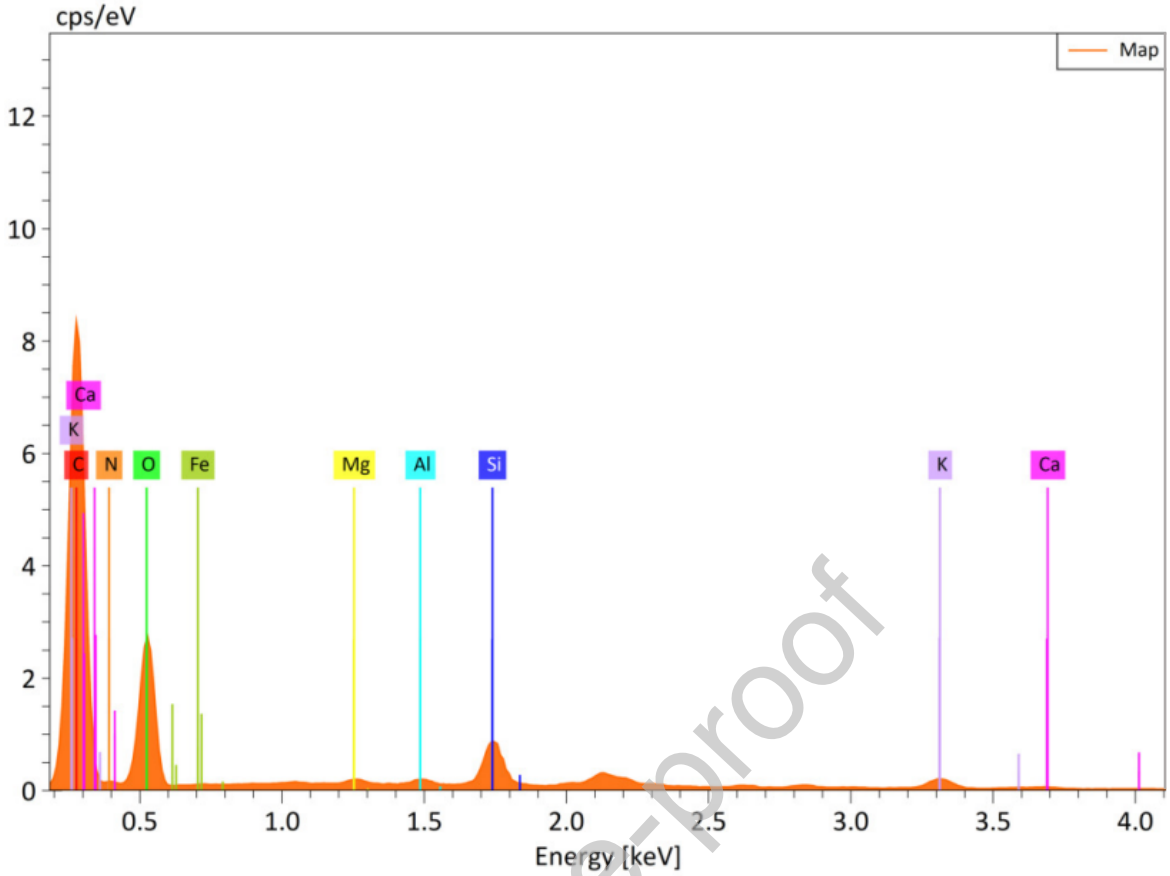

Figure 8. EDX mapping of RHB

2.4. Sample preparation

The principal challenge in applying MICP to expansive subgrade soils lies in the homogenization process. Due to the impermeable nature of these soils, it is essential to blend enrichment and cementation solutions directly with the soil matrix. The procedure began with air-drying and grinding the soil, followed by measuring its residual moisture content. RHB was incorporated into the soil in varying proportions (0 %, 1 %, 2 %, 3 %, 4 % by dry soil weight), with components accurately weighed and mixed dry.

Subsequently, the enrichment solution was added to achieve the soil's optimum moisture content. The mixture was then allowed to rest for 2 and 4 days in a controlled environment at 27±2 °C and 65±5 % humidity, facilitating the urea hydrolysis process. After this mellowing phase, the reduction in the weight of the enrichment solution was measured, and a corresponding amount of the cementation solution was added to maintain the optimum moisture level. Table 5 shows the composition of the samples prepared for this research.

For each combination of RHB content and mellowing period, three replicate specimens were prepared and tested. The results reported represent the average values of these replicates. Error bars indicating one standard deviation are included in the relevant figures.

Table 5. Composition of the samples prepared in this research

Sample ID	Mellowing Periods (Days)	Rice Husk Biochar (wt%)
M0B0 (Raw)	0	0.0
M0B1	0	1.0
M0B2	0	2.0
M0B3	0	3.0
M0B4	0	4.0
M2B0	2	0.0
M2B1	2	1.0
M2B2	2	2.0
M2B3	2	3.0
M2B4	2	4.0
M4B0	4	0.0
M4B1	4	1.0
M4B2	4	2.0
M4B3	4	3.0
M4B4	4	4.0

2.5. Experimental investigations

2.5.1. Strength tests

The unconfined compression test was conducted in line with ASTM D5102 (2009). To ensure precision, the specimen was carefully positioned on the lower platen, minimizing contact with the upper platen. Axial force and deformation were continuously measured as the test progressed at a constant deformation rate of 1 % per minute until failure. Following these steps, the compressive strength of the specimen was assessed using Eq. 7.

$$\sigma_c = \frac{P}{A} \tag{7}$$

Here, σ_c represents compressive strength, P the peak load, and A the cross-sectional area of the sample.

The split tensile strength test was performed according to ASTM C496 (2011). Cylindrical specimens were positioned horizontally within the testing apparatus and subjected to failure at a 0.5 mm/min displacement rate. The split tensile strength, σ_T, was determined using Eq. 8.

$$\sigma_T = \frac{2P}{\pi t d} \tag{8}$$

The California bearing ratio (CBR) test was conducted in line with ASTM D 1883 (2021). Prior to testing, the samples were soaked for four days under a 5 kg surcharge. CBR testing was then performed at 1.25 mm/min using a loading frame equipped with a 50-mm diameter plunger.

In addition, the resilient modulus of the treated specimens was estimated from the CBR penetration resistance values using the empirical relationship recommended by IRC-37 (2012), as given in Eq. (9).

$$M_r = 17.6 \times (CBR)^{0.64} \quad (9)$$

Where, M_r denotes the resilient modulus of the soil in MPa, while CBR refers to the California Bearing Ratio in percentage.

2.5.2. Shrink-swell tests

1D swell tests were conducted on both untreated and treated soil samples following ASTM D4546 (2021), Method A guidelines were followed to evaluate the swelling potential and swell pressure.

Free swell index tests were performed in line with IS: 2720 (Part XL) (1991). Two samples of oven-dried soil, each weighing 10 grams and sieved to 425 microns, were transferred into individual 100 ml graduated cylinders—one filled with kerosene and the other with deionized water. After removing air bubbles through gentle stirring, the cylinders were allowed to settle for at least 24 hours to achieve volume stabilization. The final soil volumes in both cylinders were recorded. The volume in the kerosene-filled cylinder, where kerosene prevents swelling, was noted as the initial volume (V_k). The expanded volume in the distilled water-filled cylinder represented the free swell volume (V_d). The free swell index (FSI, %) was then measured using Eq. 10:

$$\boldsymbol{FSI}\ (\%) = \frac{\boldsymbol{Vd - Vk}}{\boldsymbol{Vk}} \times \mathbf{100} \quad (10)$$

Linear shrinkage tests were conducted on both unstabilized and stabilized soil specimens following BS 1377 (1990).

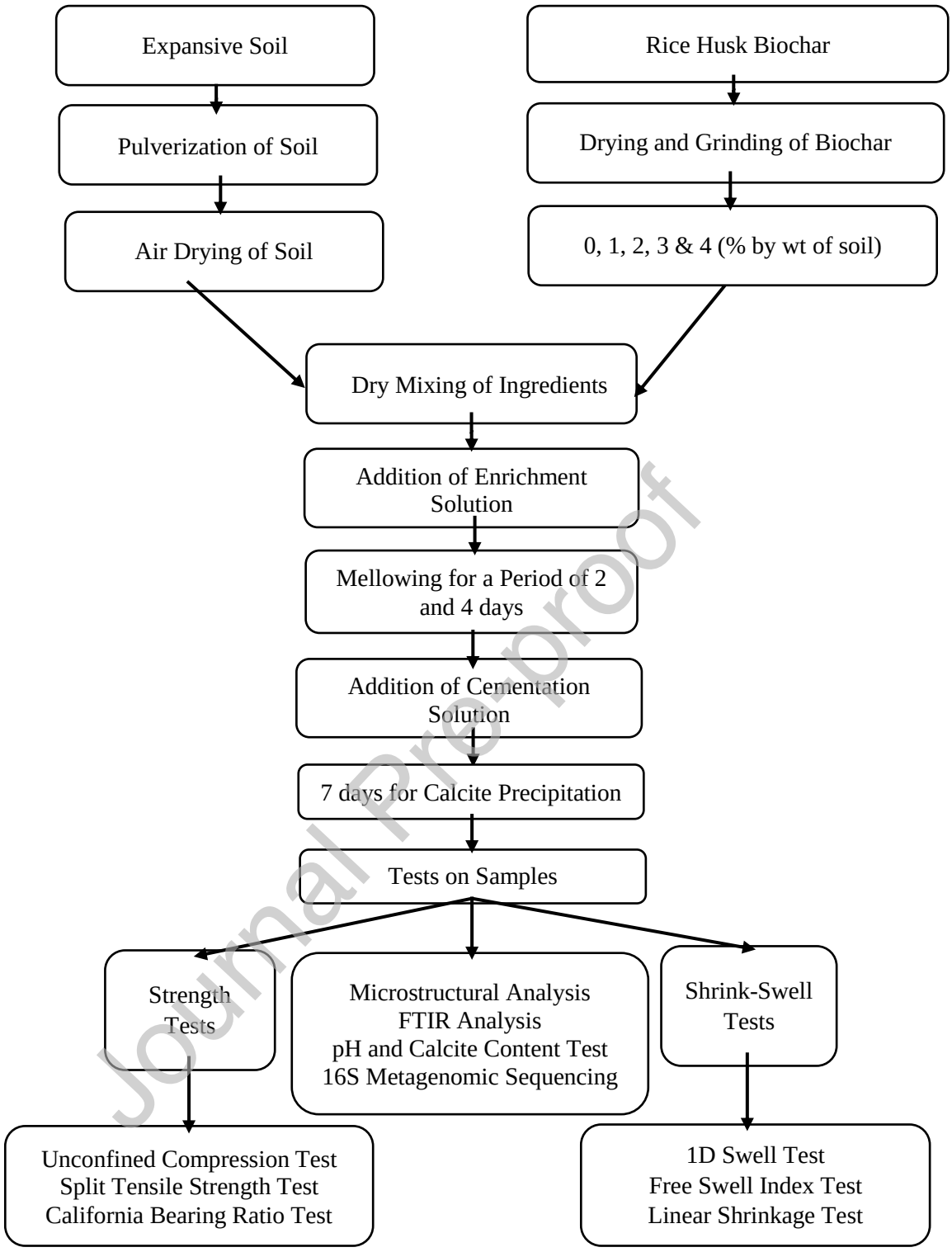

Figure 9. Outline of the preparation of samples and test plan

2.5.3. pH and Calcite content measurement

The pH levels of the samples were measured according to ASTM D 4972 (2019) to assess the chemical alterations in the expansive subgrade soil resulting from biocementation. For pH measurement, 10 grams of both stabilized and unstabilized soil specimens, collected from the broken specimens of the strength tests, were thoroughly stirred

with 10 mL of deionized water in a 20 mL vial. This mixture was then agitated using a mechanical shaker for one hour. Afterward, the pH was evaluated by fully immersing the pH electrode into the liquid portion of the slurry.

The evaluation of chemical alterations in expansive subgrade soil involved assessing the calcite content following ASTM D 4373 (2021). Around 10 grams of soil was taken from the broken UCS samples and oven-dried at 110 ± 5 °C for 24 hours. Afterwards, the sample was pulverized until it passed through a No. 40 (0.425 mm) sieve. Then, 1 ± 0.01 grams of the pulverized sample was placed inside the reactor. Next, 20 ± 2 mL of 1N hydrochloric acid solution was added into the chamber in an acid container. The reactor was sealed with a top cap, and the pressure relief valve was closed. The chamber was then tilted to mix the acid with the specimen and shaken. The calcite content was determined from the pressure in the dial gauge, which indirectly indicated the amount of CO_2 produced, using the calibration curve of the apparatus.

2.6. Microstructural analysis

In this study, microstructural characteristics were carefully examined using scanning electron microscopy (SEM). Analyses were conducted on a Sigma 360 VP FESEM system (ZEISS), which employs an electron gun to generate electrons that are focused into a beam via magnetic lenses. The beam scans the specimen in a grid pattern, while detectors capture surface emissions to produce high-resolution images. Both control sample and soils treated with MICP bio-stimulation and RHB were analyzed. Preparation of specimen includes oven-drying for 24 hours, followed by sectioning into around 0.5 cubic inch pieces, which were then placed in the chamber. Imaging was done at a voltage of 3 kV and a distance of 5–7 mm to obtain detailed microstructural observations. Additionally, ATR-FTIR spectroscopy was employed to investigate chemical bond alterations induced by stabilization. KBr pellet samples were scanned using a PerkinElmer ATR-FTIR spectrometer over a range of 500–4000 cm^{-1}. Figure 10 illustrates the experimental setups used for these analyses.

(a)

(b)

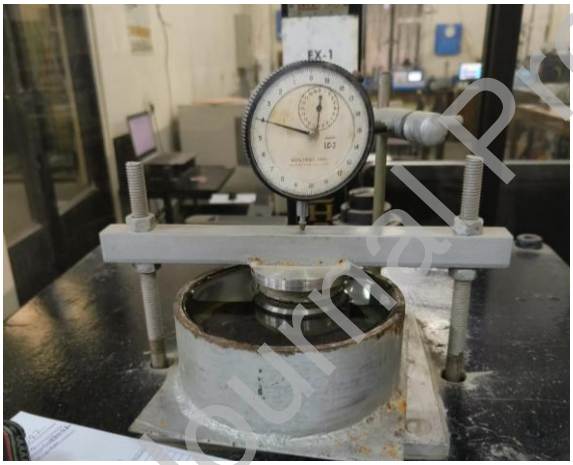

(c)

(d)

(e)

(f)

(g)

(h)

Figure 10. Test setups for (a) UCS test, (b) STS test, (c) 1D swell test, (d) Linear shrinkage test, (e) Calcite content test, (f) CBR test, (g) SEM-EDX, and (h) FTIR

2.7. 16S Metagenomic Sequencing

16S metagenomic sequencing was performed on three different soil specimens: untreated soil (M0B0), soil treated with only MICP bio-stimulation with a 4-day mellowing period (M4B0), and soil treated with both 4-day mellowing period MICP bio-stimulation and optimal RHB content (M4B2).

A total of 250 mg of soil was processed using the DNeasy PowerSoil Pro Kit (Figure 11 a). DNA purity was evaluated with a Nanodrop spectrophotometer (Figure 11 b), yielding a 260/280 ratio of 1.8, indicative of high-quality DNA with minimal protein contamination, and a 260/230 ratio of 2.0, confirming negligible interference from carbohydrates or other organic compounds. DNA quantification was performed using a Qubit 4.0 Fluorometer, with the working solution prepared by mixing Qubit reagent and buffer in a 1:200 ratio, followed by measurements of both samples and standards in appropriate assay tubes.

For library preparation, the 16S Barcoding Kit 24 V14 (SQK-16S114.24) was employed. Genomic DNA samples (10 ng each) were transferred into 0.2 ml PCR tubes and diluted to a final volume of 15 µl with nuclease-free water (Figure 11 c). PCR reactions were set up by combining the DNA samples with LongAmp Hot Start Taq 2X Master Mix. Barcodes from a 24-well plate were thawed, mixed, and added to the PCR tubes (Figure 11 d). The amplification protocol consisted of denaturation, annealing, and extension steps. Post-amplification, EDTA was added to terminate the reaction, followed by incubation. Each barcoded sample was quantified using a Qubit fluorometer, pooled in equimolar amounts, and purified using AMPure XP beads. The eluted DNA library was subsequently quantified, diluted, and combined with a diluted Rapid Adapter mixture, followed by incubation. Finally, after priming, the prepared DNA libraries were sequenced on the MinION platform (Figure 11 e).

Analysis of the 16S rRNA amplicons generated by Oxford Nanopore Technologies (ONT) was performed using a custom bash script that served as a wrapper for QIIME2 analysis (Figure 11 f).

(a) (b)

(c) (d)

(e) (f)

Figure 11. Test setup for (a) Preparation for DNA extraction, (b) Spectrophotometer, (c) Library preparation, (d) PCR machine, (e) Oxford MinION, and (f) Illumina 16S metagenomic sequencing platform

The script began by parsing command-line arguments for the input directory, reference sequences, classifiers, and the number of CPU threads. FASTQ files were concatenated, and the reads were demultiplexed and trimmed. Quality control was maintained by filtering and trimming reads to a length of 1400 base pairs. Dereplication of sequences and detection and filtering of chimeric sequences were accomplished using various QIIME2 plugins. Sequences were aligned using mafft, then masked and filtered for highly variable positions using QIIME2 functions. Unrooted and rooted phylogenetic trees were generated using FastTree. Taxonomy assignment was performed using a pre-trained classifier, and taxonomy-assigned sequences were filtered to discard non-specific taxa. The data were exported in Biom format for further analysis in Phyloseq. Taxonomic diversity was visualized using the R package microViz.

3. Results and discussions

3.1. Strength properties

3.1.1. Unconfined compressive strength

Figure 12 illustrates the axial stress-strain behavior, whereas Table 6 presents the unconfined compressive strength (UCS) values. The specimen ID "M0B0" refers to the unstabilized control specimen. For other samples, "M" followed by a number indicates the mellowing period in days after adding the enrichment solution, and "B" followed by a number specifies the percentage of RHB by weight. The unstabilized sample exhibited a UCS value of 0.072 MPa. The UCS tests done on soil specimens treated with varying portions of RHB indicate that initially, the strength of the soil increases with increasing RHB content, which aligns with the findings of Wani et al. (2022). This enhancement can be linked to the fine RHB particles filling the soil pores and the biochar functioning as a pozzolanic material (Morales et al., 2021). Moreover, the higher angularity and sharp edges of the RHB increase friction and interlocking between the soil grains, which may also contribute to this improvement (Wani et al., 2022). However, as the RHB content increases further, UCS values decrease because of the rise in organic content and the increased amount of water absorbed by the soil. The outcomes align with the study of Wani et al. (2022) and Lu et al. (2014). This observation highlights the primary rationale for combining MICP and RHB in soil treatment. The integration of MICP helps mitigate the decrease in strength associated with higher biochar content by promoting calcite precipitation, which bridges the soil grains and enhances the soil's structural integrity.

UCS tests done on soil samples treated with MICP bio-stimulation and varying percentages of RHB demonstrated a dramatic improvement in strength. The improvement in UCS values ranges from 66 % to 106 % in stabilized samples compared to the unstabilized one. Specifically, samples stabilized solely through bio-stimulation showed a strength increase of 66 % for a 2-day mellowing period and 74 % for a 4-day mellowing period.

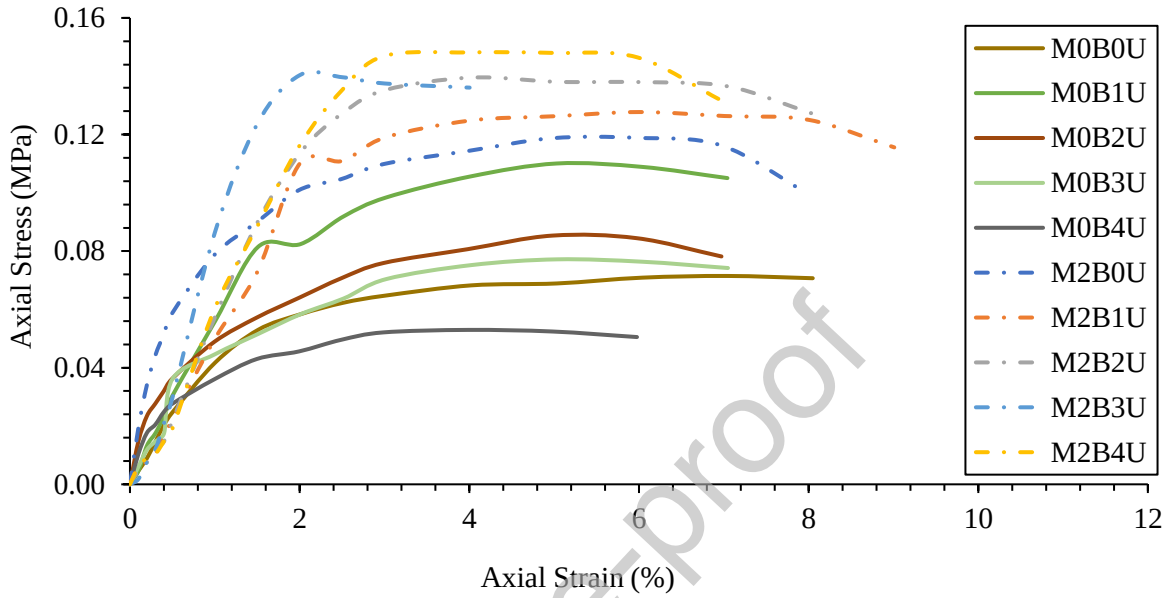

(a)

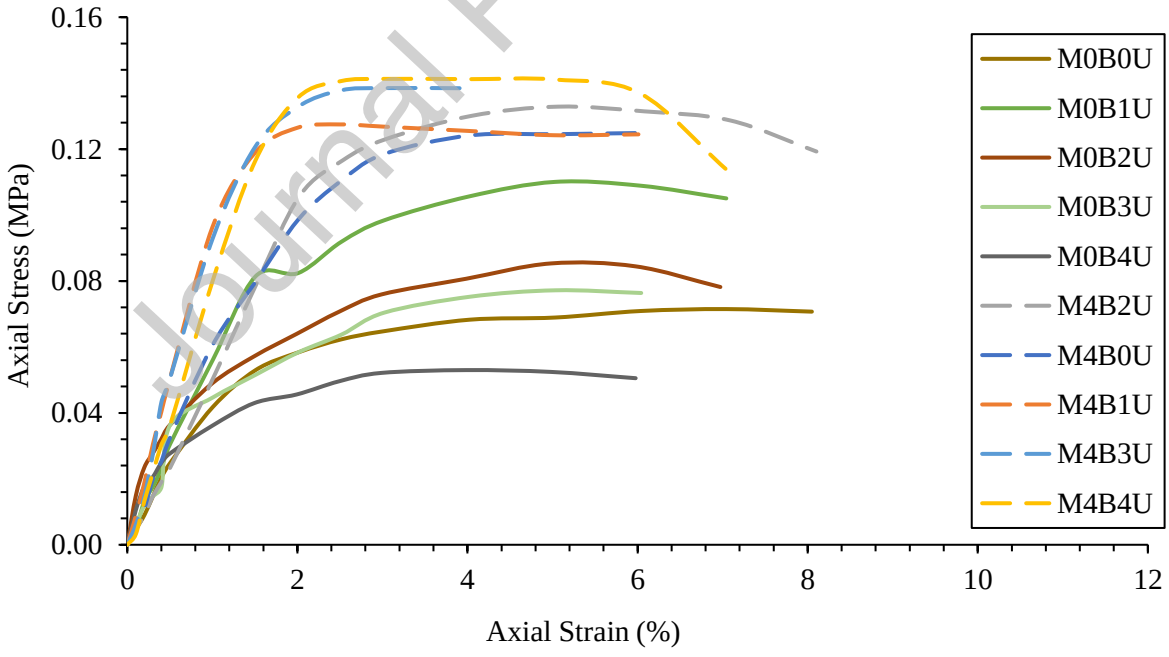

(b)

Figure 12. Axial stress-strain behaviour of (a) untreated sample and treated samples prepared considering 2-day mellowing period, (b) stabilized samples prepared considering 4-day mellowing period, from unconfined compression test

Table 6. Strength, stiffness and toughness parameters from unconfined compression and split tensile tests

Sample ID	Parameters from Unconfined Compression Test					Parameters from Split Tensile Tests				
	UCS (MPa)		Secant Modulus (MPa)	Initial Tangent Modulus (MPa)	Modulus of Toughness (kJ/m^3)	STS (MPa)		Secant Modulus (MPa)	Initial Tangent Modulus (MPa)	Modulus of Toughness (kJ/m^3)
	$\bar{x}$	σ				$\bar{x}$	σ			
M0B0	0.072	0.004	1.90	4.30	5.58	0.023	0.002	0.68	1.43	0.52
M0B1	0.110	0.006	3.65	8.55	6.26	0.014	0.004	1.41	1.60	0.24
M0B2	0.085	0.009	2.83	8.63	4.86	0.012	0.007	1.08	1.60	0.69
M0B3	0.077	0.008	2.55	5.76	4.47	0.017	0.005	1.04	1.05	0.42
M0B4	0.053	0.004	2.28	7.23	2.71	0.014	0.003	1.24	0.20	2.30
M2B0	0.119	0.004	4.20	14.66	8.17	0.045	0.009	1.63	1.96	1.39
M2B1	0.128	0.013	3.96	5.89	8.40	0.041	0.006	1.57	0.89	1.36
M2B2	0.139	0.009	5.70	4.27	6.60	0.043	0.008	1.05	0.89	0.95
M2B3	0.140	0.011	8.64	5.89	2.93	0.025	0.001	1.21	1.80	0.96
M2B4	0.148	0.005	5.80	2.90	6.87	0.025	0.004	1.18	0.89	1.25
M4B0	0.125	0.010	4.94	3.48	9.68	0.036	0.007	1.26	1.44	1.10
M4B1	0.128	0.007	9.64	9.99	4.18	0.033	0.005	1.99	1.99	0.88
M4B2	0.133	0.011	4.60	4.34	7.49	0.030	0.002	1.34	1.24	0.72
M4B3	0.139	0.010	8.05	8.56	5.78	0.029	0.006	0.76	1.59	0.92
M4B4	0.141	0.008	7.77	10.05	5.75	0.021	0.003	0.69	0.54	1.96

The primary mechanism behind this strength enhancement is calcite precipitation via the MICP bio-stimulation process. Indigenous soil bacteria, when stimulated, produce calcite that serves as a binding agent, filling the soil pores and enhancing cohesion. This calcite formation is crucial for the observed improved UCS values (Tiwari et al. 2021).

The integration of RHB leads to even greater strength increases, ranging from 77 % to 106 %, surpassing the results from bio-stimulation alone. The high content of amorphous silica in RHB aids in forming C-S-H bonds, known for enhancing strength (Morales et al., 2021). Moreover, RHB may boost the metabolic activity of calcite-precipitating bacteria, further improving soil strength (Behzadipour and Sadrekarimi, 2021; Singh Yadav et al., 2023; Xu et al., 2023). The synergistic effect of MICP for calcite precipitation and RHB for its pozzolanic reaction results in a composite material with superior strength characteristics. Similar studies in the field corroborate this synergistic interaction (Behzadipour and Sadrekarimi, 2021).

The integration of RHB and MICP-biostimulation in expansive soil significantly enhances its mechanical properties, as evidenced by the analysis of stress-strain curves from unconfined compression tests (Table 6). These improvements are particularly crucial for pavement applications. Enhancements in initial tangent modulus (up to about 240 %) and secant modulus (up to about 407 %) across various mellowing periods and RHB percentages indicate increased soil stiffness, suggesting an enhanced ability to withstand the stresses and deformations

associated with traffic loads. Higher toughness values (up to 7.49 kJ/m^3) correspond to a material's increased ability to absorb energy before failure, which are essential qualities for the subgrade layers in pavement construction. Also, the improvement in UCS value of the subgrade soil leads to a stronger and more durable foundation for pavement structures because a higher UCS value ensures that the subgrade can effectively bear traffic loads, reducing the stress transmitted to the upper pavement layers. This improvement minimizes pavement deformation, as the enhanced cohesion and binding of soil particles prevent excessive settlement, rutting, and fatigue cracking (Agustina and Zainorabidin, 2020). Additionally, the formation of C-S-H bonds and calcite precipitation reduces water infiltration, making the subgrade more resistant to moisture-induced weakening (Mostafa et al., 2024). As a result, the stabilized subgrade maintains its structural integrity under varying environmental conditions, ultimately extending the pavement's service life. By creating a stronger and more resilient foundation, this enhancement in UCS contributes to better pavement performance, reducing maintenance requirements and ensuring long-term durability (Ghanizadeh et al., 2024).

3.1.2. Split tensile strength

Split tensile strength is a particularly important parameter for stabilized expansive subgrade materials because these soils are inherently susceptible to tensile cracking induced by differential shrinkage during moisture loss. Such cracks originate within the subgrade and propagate upward through the pavement structure as reflective cracks, leading to moisture infiltration, accelerated deterioration, and premature failure (Paul and Islam, 2025). A stabilized subgrade with improved tensile strength can resist the onset of shrinkage cracking, thereby preserve the structural continuity of the pavement system and extend its service life (Paul et al., 2026c). The stress-strain behavior from STS tests is depicted in Figure 13, while Table 6 presents the STS values. The unstabilized sample showed an STS value of 0.023 MPa. When STS tests were performed on only RHB treated expansive subgrade soils, the tensile strength significantly decreased ranging from 26 % to 48 % as the RHB content increased. This reduction in strength is mainly because of the increased organic content and water absorption caused by the higher RHB content. Modifications in soil porosity may also have contributed to micro-crack formation, leading to a consequent reduction in tensile strength. These findings are in line with previous research by Wani et al. (2022) and Lu et al. (2014). This observation underscores the need to combine RHB with other stabilization methods, such as MICP, to mitigate the reduction in tensile strength.

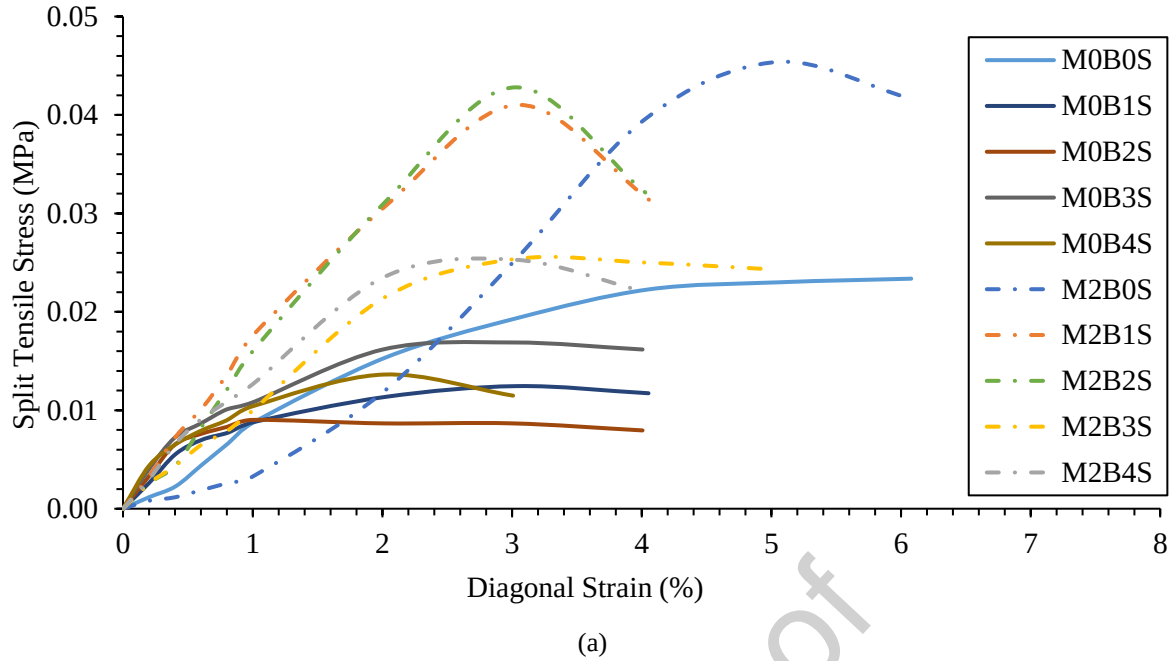

(a)

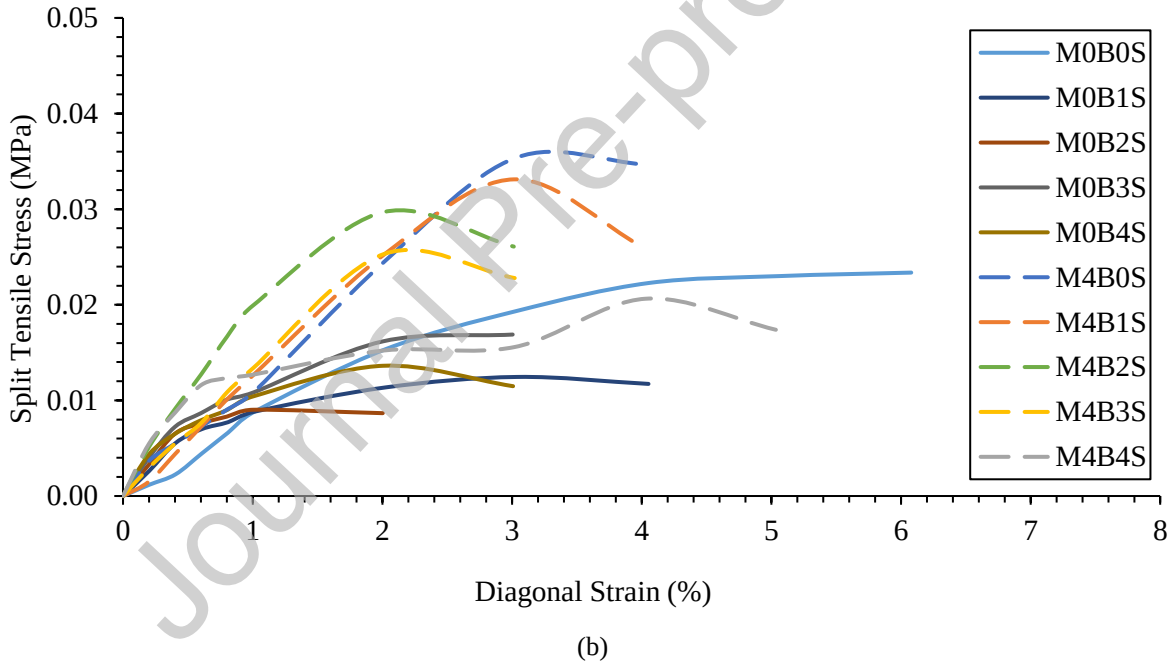

(b)

Figure 13. Diagonal stress-strain behavior of (a) untreated sample and treated samples prepared considering 2-day mellowing period, (b) stabilized samples prepared considering 4-day mellowing period, from split tensile strength test

When treated with both MICP bio-stimulation method and varying RHB contents, the improvements in STS values ranged from 31 % to 103 % compared to the unstabilized ones. The enhancement in STS can be linked to the interfacial interactions between soil grains, which are bolstered by the precipitation of calcite content due to MICP treatment and the pozzolanic activity of RHB (Morales et al., 2021). The binding of soil particles by calcite bridges likely contributes to increased tensile strength, making the material less prone to cracking. This is particularly beneficial for expansive subgrade soils, which are susceptible to significant volumetric changes with

moisture variations and could greatly benefit from increased tensile strength to mitigate cracking. The outcomes of this research align with those described by Tiwari et al. (2021), where a marked increase in STS was observed following MICP treatment. Moreover, the process of biostimulation was enhanced by the nutrition provided by RHB, and the process of calcite precipitation was enhanced by the highly porous structure of RHB (Behzadipour and Sadrekarimi, 2021; Singh Yadav et al., 2023; Xu et al., 2023).

Overall, the results present a compelling case for using MICP bio-stimulation coupled with rice husk biochar to improve tensile strength and reduce susceptibility to tensile cracking in expansive subgrade soils. While RHB decreases the shrink-swell potential, it also reduces tensile strength. This negative effect is mitigated through the application of MICP bio-stimulation. Mitigating the reduction in split tensile strength (STS) through MICP bio-stimulation and RHB incorporation has a direct impact on improving pavement performance by enhancing the structural resilience of the subgrade.

The analysis of split tensile tests from Table 6, initial tangent modulus, secant modulus and modulus of toughness parameters, underscores the improvement in stiffness and toughness of expansive soils improved with RHB and MICP-Biostimulation. The initial tangent modulus and secant modulus show notable increases in samples like M2B1 and M4B2, which indicates a more rigid soil structure capable of better distributing loads across the pavement. This increased stiffness is crucial in reducing deformations under traffic loads, enhancing the pavement's ability to endure repeated stress without significant wear. Similarly, the modulus of toughness from the split tensile tests, which quantifies the energy absorption capacity of the soil before failure, shows significant enhancements. Higher values observed in stabilized samples indicate a greater ability of the treated soil to absorb and dissipate energy, which is vital in mitigating the impact of dynamic loads. Furthermore, a higher STS value means that the subgrade is less prone to tensile cracking, which is particularly critical for expansive soils that experience significant volumetric changes due to moisture fluctuations. By increasing the tensile strength of the underlying subgrade, the likelihood of shrinkage-induced cracks is minimized, reducing the potential for reflective cracking in the pavement layers above. This improved resistance to cracking also enhances the overall load distribution across the pavement structure, preventing localized failures and ensuring greater durability under repeated traffic loading (Yan et al., 2023). Additionally, the improved tensile properties contribute to better stress absorption and dissipation, reducing the risk of premature pavement distress (Shekhawat et al., 2020). As a result, the combination of MICP bio-stimulation and RHB not only strengthens the subgrade but also enhances the long-term stability and serviceability of the pavement, ultimately leading to reduced maintenance costs and extended pavement lifespan (Ghanizadeh et al., 2024).

3.1.3. California Bearing Ratio (CBR)

Figure 14 depicts the stress penetration curves for selected specimens, including the untreated soil (M0B0), soil treated with 2 % RHB content only (M0B2), soil stabilized solely through bio-cementation for various mellowing periods (M2B0 and M4B0), and soil enhanced with both bio-cementation with a four-day mellowing period and RHB content of 2 % (M4B2). The choice of 2 % RHB content stems from its optimum performance in shrink-swell behavior analysis. Moreover, the four-day mellowing period was chosen because it showed the best performance in both strength and shrink-swell behavior analyses. Table 7 presents the soaked CBR values for these specimens. The untreated soil showed a soaked CBR of 2.5 %. The specimen treated with only the optimum RHB content (M0B2) had the same soaked CBR value of 2.5 %, indicating that optimum RHB content causes little or no change in the soaked CBR value of expansive subgrade soil. Hussain et al. (2022), Wani et al. (2022), and GuhaRay et al. (2019) have displayed that even when CBR values increase with certain treatments, the improvement is typically minimal. However, the bio-cemented specimens demonstrated significant increases in CBR values, ranging from 72 % to 88 % compared to the untreated soil, primarily due to the formation of calcite particles that effectively bind the soil particles (Tiwari et al., 2021). Notably, the specimen treated with both biostimulation and optimal RHB content (M4B2) showed a substantial 52 % improvement in CBR, outperforming the specimen treated with only RHB. Furthermore, the resilient modulus of the bio-cemented specimens, with or without biochar, ranged from 41.28 to 47.62 MPa. Regarding subgrade thickness requirements dictated by CBR values, the enhancements provided by bio-cementation and biochar frequently exceed the pavement design standards outlined by LGED (1999). For example, both the untreated soil sample (M0B0) and the soil stabilized solely with RHB, each exhibiting a CBR of 2.5 %, necessitate an improved subgrade thickness of 450 mm according to LGED guidelines. In contrast, treated samples such as M2B0, M4B0, and M4B2, which demonstrate CBR values ranging from 3.8 % to 4.7 %, permit a reduced subgrade thickness of 250 mm. Based on Bowles' classification system (Bowles, 1992), M0B0 and M0B2 are classified as "Very Poor," making them suitable only for low-strength applications. On the other hand, M2B0, M4B0, and M4B2 are assessed as “Poor to Fair”, indicating medium improvements in strength. These results indicate that the RHB-MICP treated subgrade is suitable for use beneath low-volume flexible pavements and rural road infrastructure, where the treated layer can serve as an improved subgrade or working platform, reducing the required thickness of imported granular fill. The method is also applicable to embankment fills and foundation beds for lightly loaded structures such as single-story buildings, boundary walls, and canal linings constructed on expansive soil deposits.

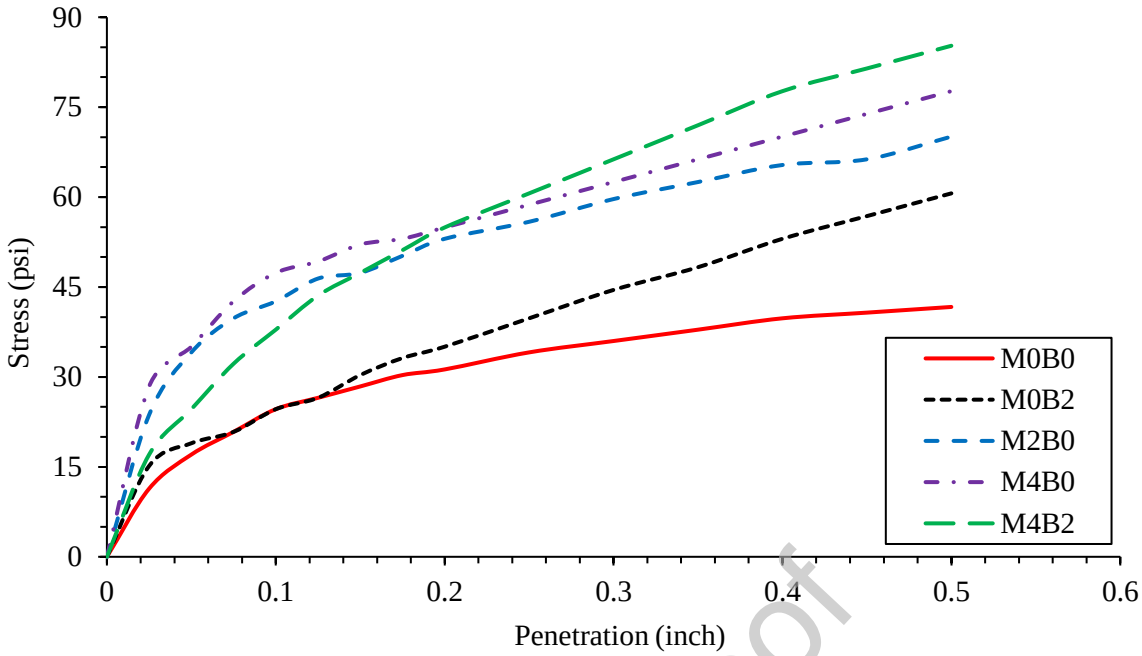

Figure 14. Stress-Penetration Curve from the soaked CBR test

Table 7. Soaked California bearing ratio (CBR) values of unstabilized and stabilized samples

Sample ID	Soaked CBR (%)		Resilient Modulus of Soil (MPa)
	$\bar{x}$	σ	
M0B0	2.5	0.27	31.33
M0B2	2.5	0.21	31.33
M2B0	4.3	0.34	44.51
M4B0	4.7	0.30	47.62
M4B2	3.8	0.19	41.28

3.2. Shrink-swell behavior

3.2.1. Free swell index

Table 8 vividly demonstrates the effectiveness of the combined use of bio-stimulation-based MICP and RHB in modifying the swell characteristics of soils. Initially, the unstabilized soil displayed an FSI value of 82.6 %. When treated with only RHB, the free swell index (FSI) value initially decreased as the RHB content increased. This reduction is due to the biochar's ability to absorb water, engage in pozzolanic reactions, and fill soil pores, thereby reducing the soil's swell potential (Morales et al., 2021; Villarreal and Wang, 2021). Moreover, the high cation exchange capacity and surface negativity of RHB allow it to counterbalance the positive charges of cations dispersed in the soil's diffused double layer (Pan et al., 2021a). However, when the RHB content exceeded 2 %, the FSI value began to rise again, indicating an optimum RHB content of 2 % for minimizing the swell potential of expansive subgrade soils. This is because when the optimum RHB content has been exceeded, unbalanced

negative charges in biochar-treated soils may repel each other, resulting in expansion at the molecular level (Villarreal and Wang, 2021). This result aligns with the previous research of Pan et al. (2021). Optimum RHB content lowers the FSI value by 93 % when compared with the unstabilized specimen.

Table 8. Free swell index values (%) of unstabilized and stabilized samples

Sample ID	Free Swell Index (%)	
	$\bar{x}$	σ
M0B0	82.6	2.4
M0B1	11.6	0.8
M0B2	5.9	0.4
M0B3	11.8	0.5
M0B4	23.5	1.1
M2B1	5.4	0.5
M2B2	2.7	0.2
M2B3	8.1	0.7
M2B4	13.5	0.9
M4B1	3.2	0.3
M4B2	1.5	0.1
M4B3	4.5	0.4
M4B4	5.7	0.5

Table 8 also shows the pronounced decrease in FSI values for the stabilized specimens achieved through the synergistic application of MICP and RHB. The stabilized specimens showed FSI values ranging from 1.5% to 13.5%, equating to reductions between approximately 84 % and 98 %. Both two-day and four-day mellowing periods demonstrated optimal results with an RHB content of 2 %. However, the four-day mellowing period yielded better outcomes than the two-day period. This extended mellowing period likely allows for more thorough interaction between the clay and the RHB, leading to improved soil stabilization and better reduction of the swell potential. The significant reduction is primarily attributed to the incorporation of RHB as previously discussed. Additionally, the calcite precipitated through the application of MICP effectively binds soil particles, reducing their ability to absorb water. The calcite formed is inherently non-expansive, promoting a cementing effect among the soil particles (Tiwari et al. 2021). The integration of RHB also complements this process by contributing extra siliceous materials, further solidifying the soil matrix (Morales et al., 2021). Therefore, the synergistic use of MICP and RHB not only mitigates the swell potential of expansive subgrade soils but also enhances their structural integrity by promoting calcite formation and providing additional siliceous material.

Reducing FSI of expansive subgrade soils enhances pavement performance by minimizing volumetric changes that cause heaving and cracking. A lower FSI ensures greater subgrade stability, reducing differential settlements and improving load distribution across pavement layers (Djellali et al., 2017). The combined effect of MICP bio-stimulation and RHB treatment strengthens the soil matrix, limiting water absorption and preventing excessive

expansion (Mostafa et al., 2024). This stabilization leads to a more durable pavement structure, reducing maintenance needs and extending service life.

3.2.2. Linear Shrinkage

The linear shrinkage (LS) test results indicate a significant decrease in LS values, indicating increased soil stability following treatment, as shown in Figure 15. Initially, the unstabilized soil showed a high LS value of 14.4 %. In contrast, samples treated with only RHB demonstrated reductions in LS ranging from 17 % to 34 % compared to the untreated specimen. Similar to the FSI results, the LS value was found to be lowest at the optimum RHB content of 2 %. This indicates that at this specific RHB content, the soil exhibits the least amount of shrinkage, aligning with the observations made for FSI. The 2 % RHB content effectively enhances the soil's properties, minimizing both its swelling and shrinkage behaviors. This optimal content provides a balanced improvement in the soil's performance, addressing issues associated with expansive subgrade soils (Villarreal and Wang, 2021). When treated with both MICP biostimulation and RHB, there was a pronounced decrease in the LS value, ranging from 75 % to 85 %, mirroring the pattern observed in the FSI value. Both the two-day and four-day mellowing periods showed better results than samples treated with only RHB, with the optimal results achieved at the 2 % RHB content. Similar to the FSI results, the M4B2 samples showed better performance than the M2B2 samples, demonstrating the superior effectiveness of the four-day mellowing period combined with the optimum biochar content. This decrease suggests that the enrichment and cementation solutions create an effective environment for bacterial growth. Additionally, the incorporation of RHB proves to be particularly advantageous. Its absorption of water and pozzolanic reaction with calcium form a compact matrix of C-S-H, further stabilizing the soil structure and decreasing its potential for shrinkage (Morales et al., 2021). Moreover, the reduction in voids between the soil particles and RHB's ability to balance the charges of expansive clay minerals, due to its high CEC and negative charges, also contribute to this pronounced decrease in LS (Pan et al., 2021a).

Reducing LS enhances pavement performance by minimizing soil contraction, which prevents the formation of cracks in the subgrade and overlying pavement layers. A lower LS value ensures greater dimensional stability, reducing the risk of shrinkage-induced pavement distress such as surface cracking and joint separation (Ikechukwu et al., 2021). This stabilization improves load-bearing capacity, prevents differential settlements, and enhances overall pavement durability (Agustina and Zainorabidin, 2020). The combined effect of MICP bio-stimulation and RHB treatment strengthens the soil structure, limiting shrinkage-related deformations and ensuring a longer-lasting, low-maintenance pavement system.

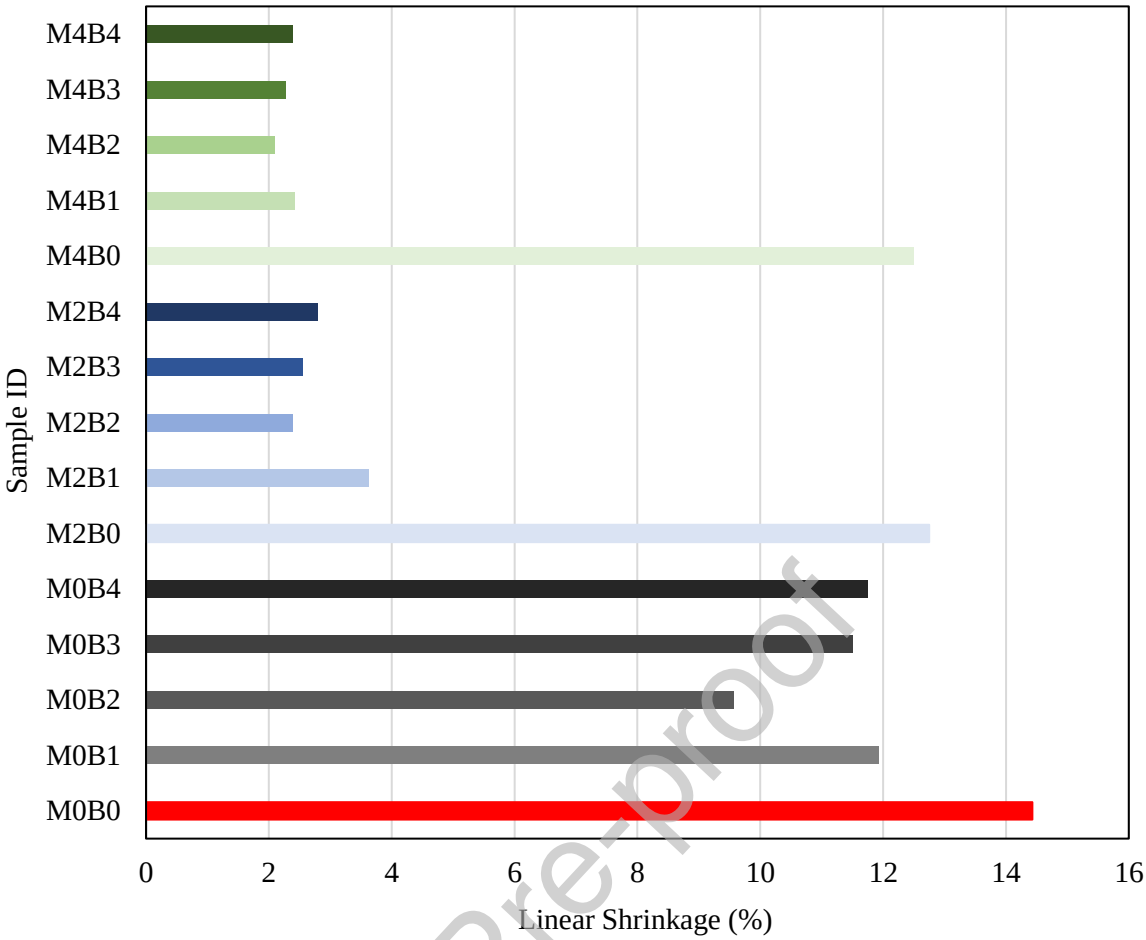

Figure 15. Linear shrinkage values for untreated and treated samples

3.2.3. Swell strain and swell pressure

Table 9 displays the outcomes from the 1D swell tests conducted on the M0B0, M0B2, M2B2, and M4B2 specimens. M0B0 untreated specimen displayed a swelling potential of 53.1 % and swelling pressure of 96.5 kPa. When treated using only RHB at the optimum biochar content of 2 %, M0B2 specimen showed a pronounced decrease in swelling potential by 21 % and swelling pressure by 64 %, as predicted from the FSI and LS values. The M2B2 specimen also exhibited a significant decrease in free swell strain by 77 % and in swell pressure by 81 %. But the M4B2 specimen showed the most significant reductions of 85 % in free swell strain and 93 % in swell pressure.

Table 9. Effect of bio-stimulation and RHB treatment on swelling characteristics from 1D Swell Tests

Sample ID	Free Swell Strain (%)		Swell Pressure (kPa)	
	$\bar{x}$	σ	$\bar{x}$	σ
M0B0	53.1	2.2	96.5	2.9
M0B2	41.8	1.8	34.5	1.2
M2B2	12.4	0.8	18.0	0.5
M4B2	8.1	0.5	6.5	0.2

These substantial decreases are primarily attributed to the bio-stimulation-induced calcite formation, which effectively binds soil particles together. Additionally, the biofilm that forms acts as a partition between the anionic clay particles and water molecules, greatly diminishing the soil's capacity to expand. These observations align with those made by Islam et al. (2020) and Tiwari et al. (2021), who noted notable reductions in 1D swell properties after applying MICP treatments stimulated by bio-stimulation. Moreover, the pozzolanic activity of RHB further amplifies the decrease in swelling pressure and strain. Adding fine RHB particles reduces the voids and the specific surface area of swelling clay minerals, facilitating the production of a C-S-H gel during the pozzolanic reaction. This gel reinforces the soil matrix and significantly reduces swelling pressure (Morales et al., 2021). The absorption of water by RHB also leads to less availability of water to the soil minerals (Behzadipour and Sadrekarimi, 2021). Additionally, the high CEC and negative charge of RHB help in balancing the positive charges of clay minerals, thereby reducing their swelling potential (Pan et al., 2021a). Thus, the integration of RHB not only complements the bio-stimulation process but also reinforces the overall stabilization of the soil, demonstrating the effectiveness of combining these treatments in controlling soil swell behavior.

Reducing free swell strain and swelling pressure significantly enhances pavement performance by minimizing subgrade expansion, which is a major cause of pavement heaving, cracking, and structural instability. When expansive soils undergo excessive swelling, they exert upward forces on the pavement, leading to surface distortions, uneven settlements, and premature failures (Ikechukwu et al., 2021). By integrating MICP bio-stimulation and RHB treatment, the formation of calcite and pozzolanic reactions effectively stabilize the soil, decreasing its potential to absorb water and swell. This stabilization ensures a more uniform and stable subgrade, preventing differential heaving and maintaining a smooth, durable pavement surface (Yan et al., 2023). Additionally, lower swell pressure reduces stress on the pavement structure, decreasing the likelihood of fatigue cracking and rutting (Djellali et al., 2017). As a result, the improved subgrade stability leads to extended pavement lifespan, reduced maintenance costs, and enhanced overall performance, making the road infrastructure more resilient to environmental and traffic-induced stresses (Ghanizadeh et al., 2024).

3.3. pH and Calcite content

Table 10 delineates the calcite content for untreated and treated soil specimens, employing this measure as a pivotal indicator of the bio-stimulation's success. The stabilized samples showed a dramatic increase in calcite content, ranging from 49 % to 215 %. This enhancement was slightly more significant in specimens that included RHB alongside MICP bio-stimulation. RHB functions as an effective support material, stimulating the metabolic

processes of calcite-forming bacteria, thereby enhancing the sustainability and effectiveness of bacterial calcite production (Behzadipour and Sadrekarimi, 2021). This increase aligns with results documented by Tiwari et al. (2021). Also, the highly porous structure of RHB helps in calcite precipitation (Behzadipour and Sadrekarimi, 2021). This underscores the efficacy of integrating RHB in bio-stimulation strategies to optimize calcite deposition in soil treatment processes. The MICP involves microbial ureolysis, resulting in ammonia synthesis, which raises the soil's pH and makes the environment more alkaline. Initially, the unstabilized soil had a pH of 6.74, but this raised to as high as 8.95 in treated specimens, as detailed in Table 10. The pH increases in specimens treated with both biostimulation and RHB varied from 28 % to 33 %, demonstrating a notable change toward alkalinity due to the MICP bio-stimulation treatment (Pan et al., 2021a).

Table 10. Calcite content (%) and pH of untreated and treated soil specimens

Sample ID	Calcite Content (% by wt)		pH	
	$\bar{x}$	σ	$\bar{x}$	σ
M0B0	0.13	0.012	6.74	0.05
M0B1	0.19	0.017	6.75	0.04
M0B2	0.2	0.018	6.97	0.07
M0B3	0.21	0.016	6.83	0.01
M0B4	0.21	0.014	6.86	0.04
M2B0	0.3	0.026	8.64	0.02
M2B1	0.32	0.028	8.70	0.07
M2B2	0.35	0.031	8.74	0.06
M2B3	0.37	0.029	8.81	0.02
M2B4	0.39	0.034	8.86	0.06
M4B0	0.34	0.027	8.79	0.05
M4B1	0.36	0.030	8.85	0.04
M4B2	0.38	0.033	8.89	0.05
M4B3	0.4	0.031	8.93	0.03
M4B4	0.41	0.036	8.95	0.03

3.4. Fourier transform infrared (FTIR) analysis

FTIR test was conducted on both the untreated (M0B0) and the treated specimens (M0B2 and M4B2), as depicted in Figure 16. The spectra revealed prominent absorption bands at 1382 cm^{-1}, characteristic of the C-O bonds found in calcium carbonate, primarily in the M4B2 specimen (Li et al., 2018b). This characteristic peak was absent in the unstabilized specimen. Furthermore, the IR peak at around 3620 cm^{-1} established the existence of montmorillonite in the untreated soil, and the presence of illite's hydroxyl group were evident in the IR band ranging from 3018 to 3702 cm^{-1} (Tiwari et al., 2021; Tiwari and Satyam, 2022). The detection of quartz was clear at IR peaks of 994, 779, and 688 cm^{-1}. Peaks at 687 and 770 cm^{-1}, corresponding to the Si–O stretching band in C-S-H, were also observed (Madadi and Wei, 2022).

The FTIR results provide direct chemical evidence linking the observed mechanical improvements to specific binding phases formed during treatment. The C-O absorption band at 1382 cm^{-1} in the M4B2 specimen confirms the presence of calcite precipitated through the MICP process, which acts as a cementing agent at inter-particle contacts, contributing to the measured increases in UCS (up to 106%) and STS (up to 103%). The Si-O stretching bands at 687 and 770 cm^{-1} indicate the formation of C-S-H gel through the pozzolanic reaction of amorphous silica in RHB with calcium ions. C-S-H gel is a well-established binding phase in cementitious systems that enhances both cohesion and stiffness (Madadi and Wei, 2022). The simultaneous formation of these two binding phases in the M4B2 specimen, which is absent in the untreated M0B0 specimen, explains the superior mechanical performance of the combined RHB-MICP treatment compared to either treatment applied individually.

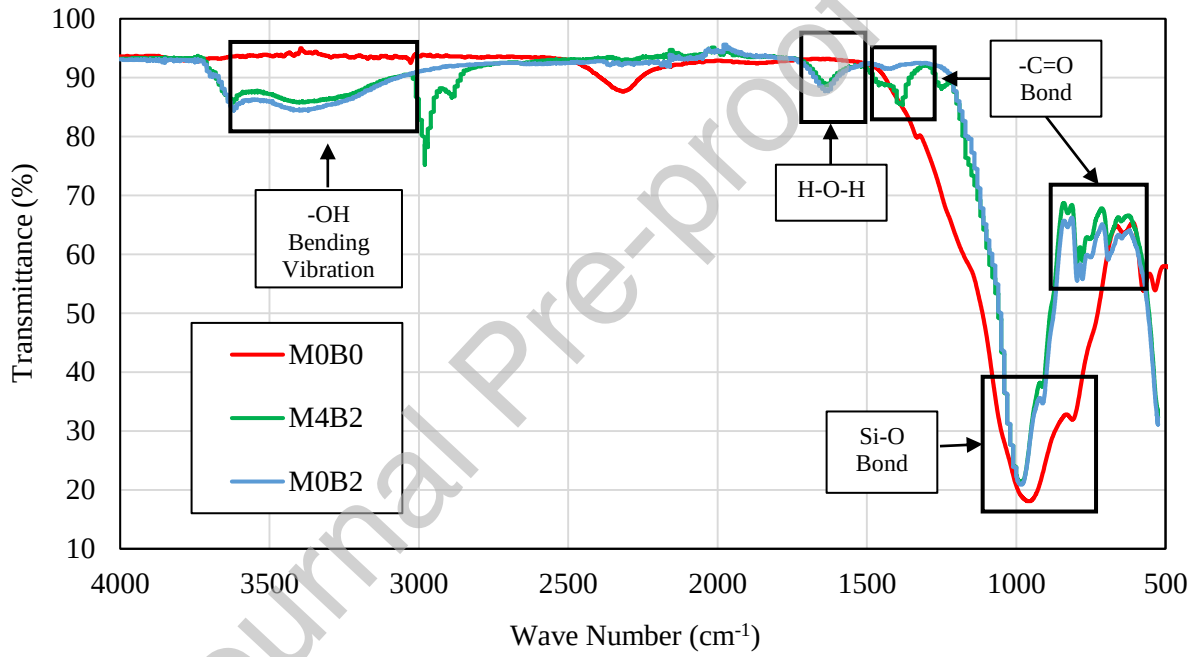

Figure 16. Comparative FTIR spectra of untreated soil – (a) M0B0 and treated soil – (b) M0B2, and (c) M4B2

3.5. Scanning electron microscopy (SEM) with Energy Dispersive X-ray (EDX) analysis

SEM analysis was conducted to evaluate the impact of MICP treatment combined with RHB on expansive subgrade soil, as illustrated in Figure 17. Figure 17 (a) proves the existence of large voids and fissures in the raw expansive subgrade soil, reflective of a weakly consolidated matrix with numerous monolithic clay clumps and fine particulate matter (Li et al., 2021). In M2B0 and M4B0 specimens (Figure 17 b, d), there is a decrease in voids and fissures due to the production of calcite crystals. This calcification, pronounced in Figure 17 (c-e), strengthens the microstructure through the development of a calcite coating that provides matrix support (Xiao et

al., 2018; Su et al., 2022; Yu et al., 2022). Consequently, the specific surface area of the expansive clay minerals is decreased, and the calcite deposited on soil particles limits soil–water interactions (Tiwari et al. 2021). For RHB-treated specimens M0B2 and M4B2, as shown in Figure 17 (b) and Figure 17 (e), respectively, adsorption and cation exchange between the RHB and soil minerals result in a reduced pore radius and the development of interconnected joints featuring new, sharper edges (Pan et al., 2021a). Additionally, the formulation of C-S-H gel results from the pozzolanic reaction of RHB (Paul et al., 2023). This reaction leads to a more interconnected soil matrix, resulting in improved strength and shrink-swell behavior.

The EDX mapping of the sample M4B2 in Figure 18 reveals that the specimen predominantly consists of the elements carbon, oxygen, silicon, calcium, and aluminum. The specimen has undergone bio-cementation and RHB treatment, exhibiting a marked increase in calcium concentration. This elevated calcium content is indicative of successful calcite precipitation facilitated by the MICP process.

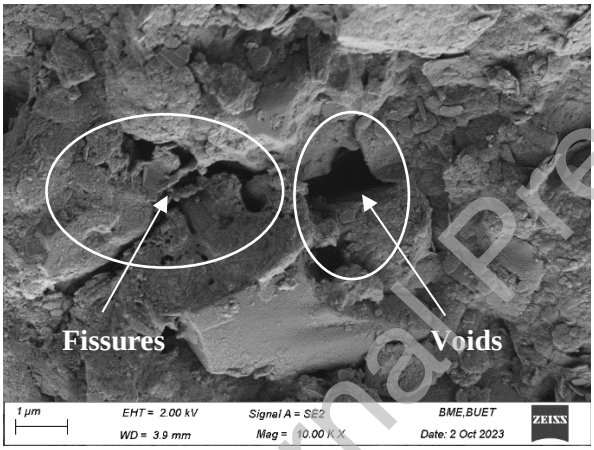

(a)

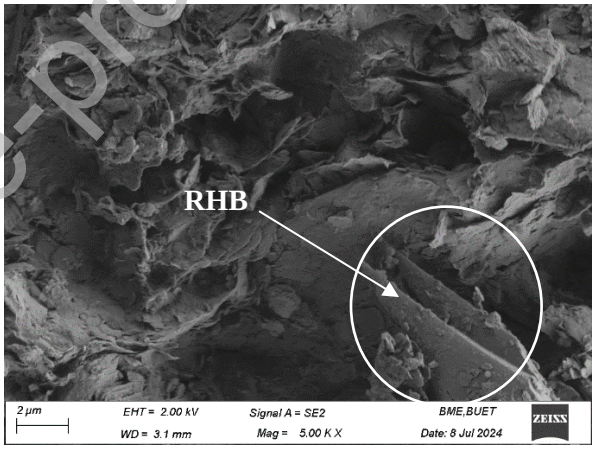

(b)

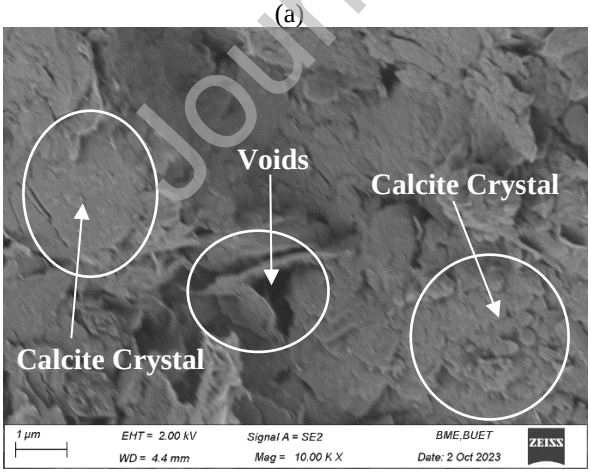

(c)

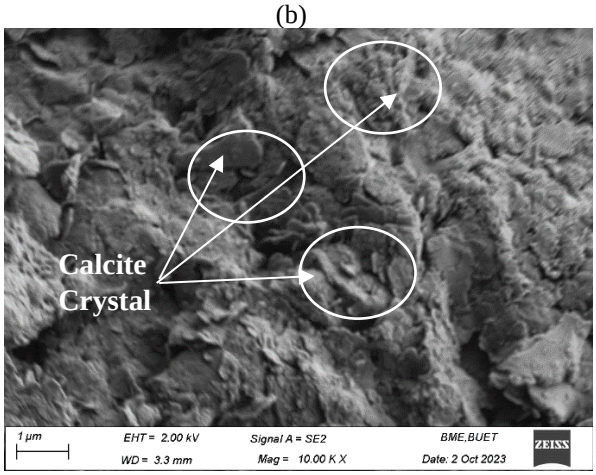

(d)

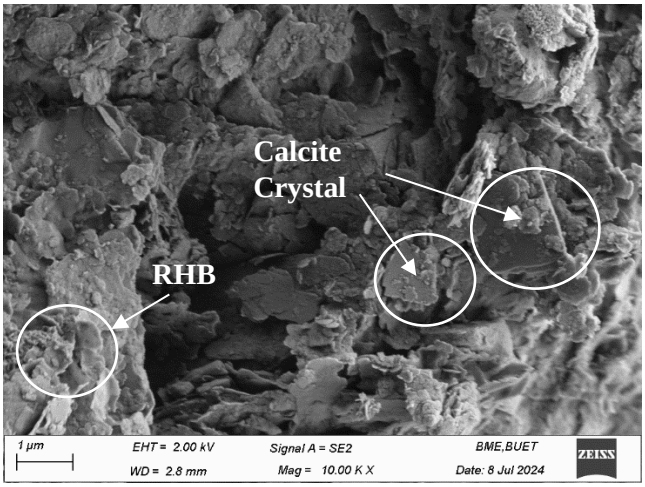

(e)

Figure 17. SEM images of (a) M0B0, (b) M0B2, (c) M2B0, (d) M4B0, and (e) M4B2

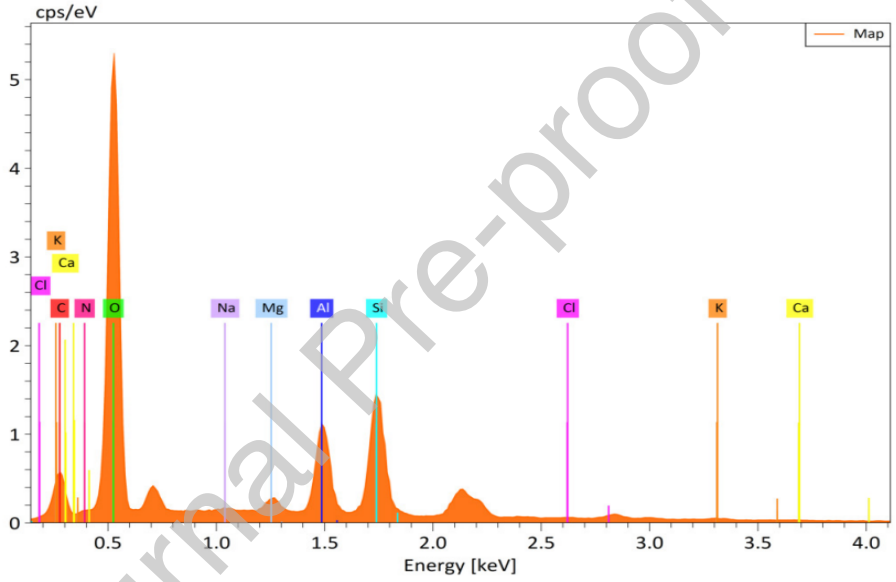

Figure 18. EDX mapping of M4B2

Here, the SEM observations can be directly correlated with the mechanical test results. The large voids and fissures visible in the untreated M0B0 specimen (Figure 17a) correspond to its low UCS (0.072 MPa) and high free swell strain (53.1%), as these discontinuities serve as planes of weakness under compression and pathways for water ingress during swelling. In the MICP-treated specimens (M2B0, M4B0), calcite crystals deposited at particle contacts bridge adjacent grains, consistent with the 66% to 74% improvement in UCS observed for these specimens. The M4B2 specimen, which demonstrated the best overall performance across all tests, shows a distinctly denser and more interconnected microstructure compared to the MICP-only specimens. The gel-like coating visible on particle surfaces in Figure 17(e) is consistent with C-S-H formation from the pozzolanic reaction, providing an additional binding phase that supplements the calcite bridges. This denser matrix with

reduced void space directly explains the 93% reduction in swell pressure observed for M4B2, as fewer and smaller pore channels limit water access to the expansive clay minerals. The progressive microstructural densification from M0B0 through M4B0 to M4B2 thus mirrors the progressive improvement in mechanical and shrink-swell performance measured across the same specimen sequence.

3.6. Analysis of 16S Microbial Community

Species-level taxonomic abundance was derived from 16S metagenomic sequencing data for three specimens: the unstabilized control (M0B0), the specimen stabilized solely through bio-cementation with a four-day mellowing period (M4B0), and the optimally stabilized specimen (M4B2), which demonstrated the best performance in shrink-swell behavior analysis. These results are depicted in Figure 19 (a). The M0B0 specimen exhibited a diverse microbial population, where Actinobacteria phylum dominated; however, bio-stimulation with MICP led to a predominance of urease-positive phyla, particularly Firmicutes and Proteobacteria (Figure 19 b).

In the unstabilized M0B0 specimen, the relative abundances of Firmicutes and Proteobacteria were 26.46% and 5.97%, respectively (Figure 19 c). Following bio-stimulation with a four-day mellowing period, their relative abundances increased to 44.43% and 19.69% in the M4B0 specimen. In the M4B2 specimen, the relative abundance of Firmicutes further increased to 53.59%, while Proteobacteria levels remained the same as the M4B0 specimen. At the genus level, the sequencing data reveal that several well-characterized urease-producing genera were enriched following bio-stimulation. Within the Firmicutes phylum, *Clostridium*, *Bacillus*, *Lysinibacillus*, and *Staphylococcus* were identified as dominant genera in the treated specimens. *Bacillus* and *Lysinibacillus* are among the most extensively studied urease-producing genera in MICP research, with documented capacities for high-rate urea hydrolysis and calcite precipitation in soil environments (Ekprasert et al. 2020; Wang et al. 2023). Within the Proteobacteria phylum, Enterobacter was identified as a notable urease-positive genus (Graddy et al., 2018). These genera catalyze the hydrolysis of urea into ammonia and carbonic acid through urease enzyme production. The ammonia raises the local pH, creating alkaline conditions favorable for carbonate ion formation, while the introduced calcium from the cementation solution combines with carbonate ions to precipitate calcite. This process is directly reflected in the measured pH increase from 6.74 to 8.95 and the calcite content increase of up to 215% in treated specimens.

The further enrichment of these urease-positive genera in the M4B2 specimen compared to M4B0 indicates that RHB actively promotes microbial metabolic activity beyond the baseline stimulation provided by the enrichment

solution alone. The addition of RHB, rich in organic carbon, phosphorus, and ammonium nitrogen, likely provided essential nutrients that fuel bacterial growth and urease enzyme production (Prendergast-Miller et al., 2011; Romdhane et al., 2019; Wang et al., 2015; Jang and Jia, 2020). The porous microstructure of RHB also provides protected habitats for bacterial colonization, shielding them from competition and environmental stress (Behzadipour and Sadrekarimi, 2021). This enhanced microbial activity translates directly to greater calcite precipitation, as confirmed by the higher calcite content in M4B2 (0.38 wt%) compared to M4B0 (0.34 wt%), and consequently to superior mechanical and shrink-swell performance. The M4B2 specimen, which exhibited the highest relative abundance of urease-positive phyla (Firmicutes: 53.59%, Proteobacteria: 19.69%), also demonstrated the best performance in free swell index reduction (98%), swell pressure reduction (93%), and UCS improvement (85%). This consistent pattern across microbiological, chemical, and mechanical indicators provides strong evidence that the enhanced bio-stimulation facilitated by RHB is the primary driver of the synergistic stabilization effect observed in this study. These findings address a notable gap in the existing MICP literature, where treatment effectiveness has typically been inferred from macroscopic indicators such as pH and calcite content without characterizing the underlying microbial community response.

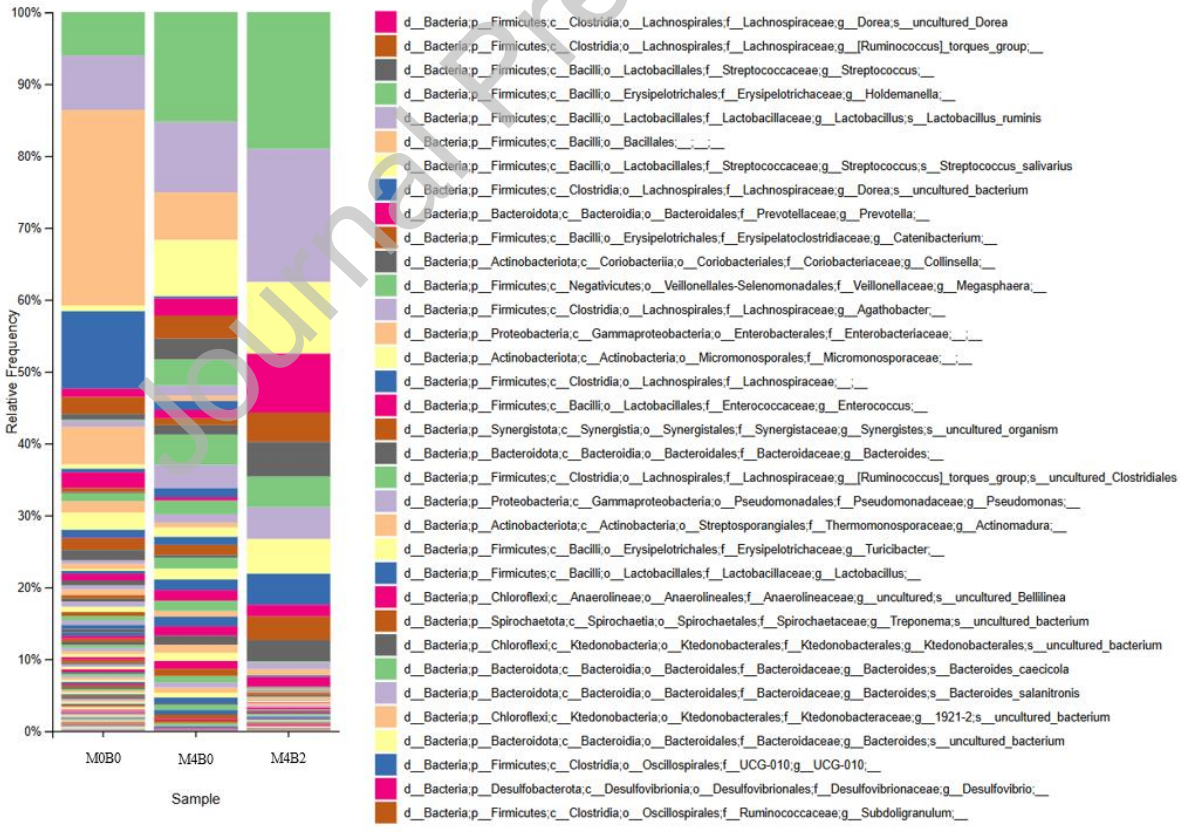

(a)

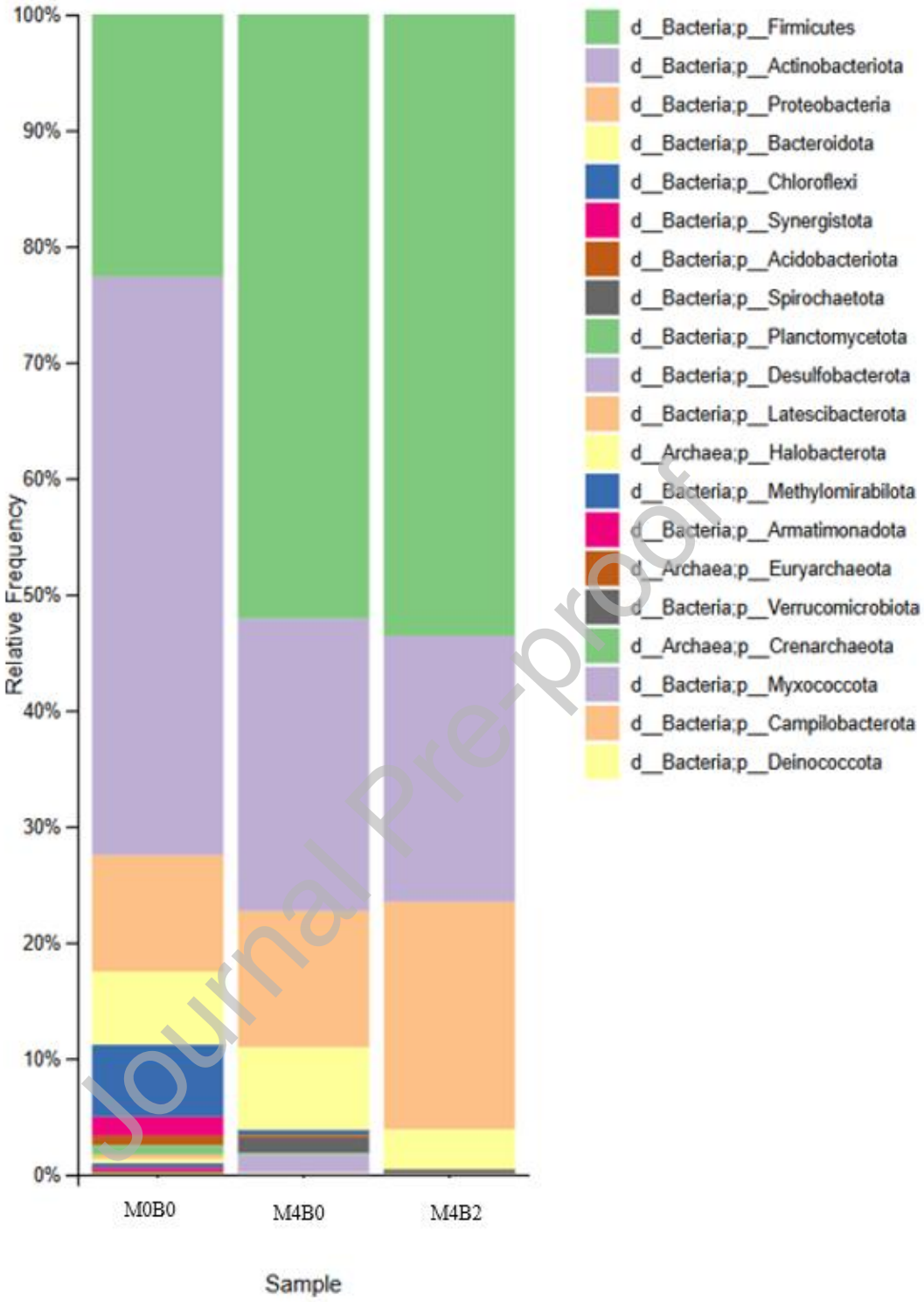

(b)

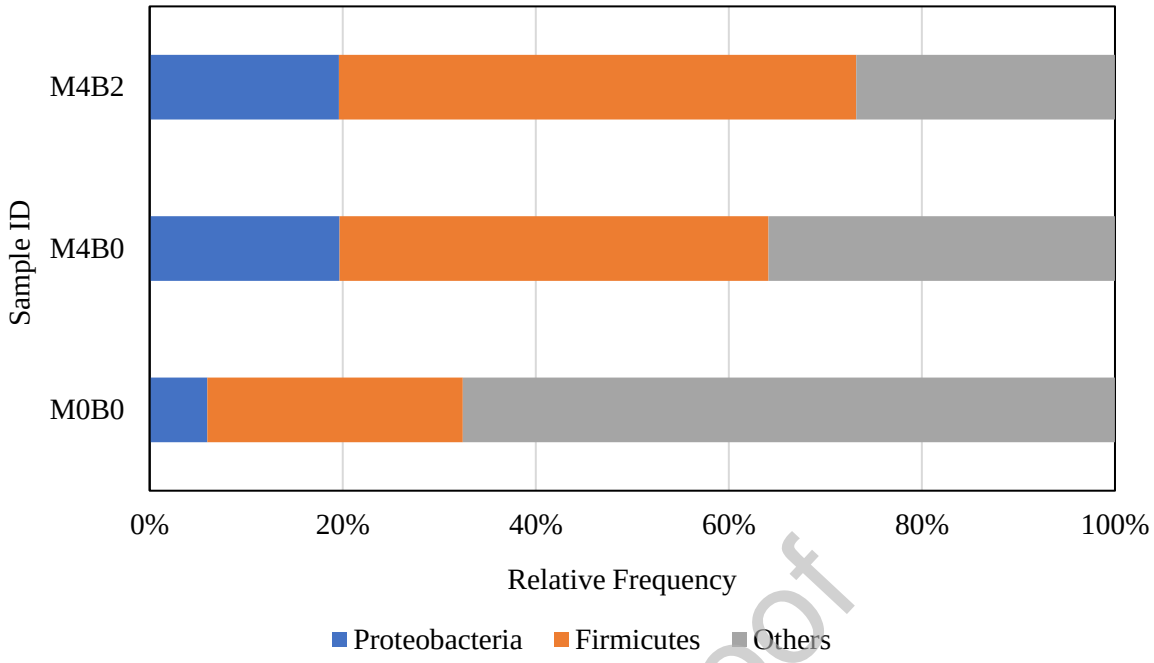

(c)

Figure 19. Analysis of 16S microbial communities- (a) Species level distribution frequencies, (b) Phylum level distribution frequencies, (c) Relative abundance of urease positive phyla and other phyla

3.7. Comparative Performance Analysis with Previous Studies

To evaluate the practical advantages of the proposed RHB-MICP bio-stimulation method relative to existing stabilization approaches, the mechanical and volumetric performance is compared with results from the literature (Table 11). The M4B2 UCS of 0.133 MPa (85% improvement) is comparable to other MICP bio-stimulation studies: Tiwari et al. (2021) reported 0.068 to 0.225 MPa, and Islam et al. (2020) achieved 0.15 to 0.40 MPa. The STS of 0.030 MPa falls within the bio-cementation range of 0.024 to 0.325 MPa (Tiwari et al. 2021) and is comparable to fiber-reinforced systems (0.03 to 0.06 MPa; (Nezhad et al., 2021)). The soaked CBR improvements of 52% to 88% are comparable to the 84% reported by Paul and Islam (2025). While these strength values are lower than cement-based systems (0.96 to 2.36 MPa; (Paul et al., 2025a)), they are appropriate for the intended application in low-volume pavement subgrades, where volumetric control rather than absolute strength is the primary design requirement.

The most notable performance is in volumetric stability, where the observed reductions are among the largest reported in the comparative literature and can be attributed to three complementary mechanisms operating simultaneously in the RHB-MICP system. First, MICP-derived calcite binds soil particles together and forms a biofilm barrier between clay surfaces and water molecules, directly limiting hydration of expansive minerals, as

also reported by Tiwari et al. (2021) and Islam et al. (2020). Second, the pozzolanic reaction of amorphous silica in RHB (72.11% SiO_2) with calcium ions produces C-S-H gel, confirmed by the Si-O stretching bands at 687 and 770 cm^{-1} in FTIR analysis (Section 3.4), which fills pore spaces and further restrains volumetric changes. Third, the high cation exchange capacity and surface negativity of RHB counterbalance positive charges in the clay diffuse double layer, reducing the electrochemical driving force for swelling (Pan et al., 2021b). This dual cementation mechanism (calcite + C-S-H) explains why the present reductions, FSI from 82.6% to 1.5% (98%), swell pressure from 96.5 to 6.5 kPa (93%), linear shrinkage from 14.4% to 2.2% (85%), exceed those achieved by MICP alone and approach cement-based performance (Table 11).

Recent studies on industrial waste-assisted MICP further contextualize the present findings. Dhorey et al. (2025a) demonstrated that combining industrial wastes (red mud, GGBS, fly ash, silica fume) with MICP using *Methylobacterium radiotolerans on* black cotton soil yielded UCS improvements of up to 192% over untreated soil, consistently outperforming industrial waste alone. Dhorey et al. (2025b) achieved UCS up to 0.971 MPa and STS up to 0.339 MPa with 15% red mud and MICP, while Dhorey et al. (2025c) optimized the MICP process via response surface methodology, reaching UCS of 1.739 MPa, the highest reported for MICP-treated expansive soil. Although none reported shrink-swell data, these studies confirm that industrial waste-assisted MICP effectively improves strength, while the present work complements this by providing comprehensive shrink-swell characterization alongside 16S metagenomic sequencing. Regarding enzyme-induced approaches for expansive soils, Mehmood et al. (2025) achieved UCS up to 0.50 MPa and CBR up to 16.1% using EICP with eggshell powder, but swell pressures remained high (10 to 250 kPa). Li et al. (2025) reported swell pressures of 121 to 168 kPa with soybean-urease SICP, with linear shrinkage reduced to 2.6%. Paul et al. (2026) investigated a hybrid EICP-sodium alginate biopolymer approach on the same expansive soil type used in the present study, achieving UCS up to 0.232 MPa (222% improvement) and swell pressure as low as 2.02 kPa (98% reduction) at 0.67% sodium alginate content, with FSI declining from 100% to 4.5%. These EICP results demonstrate that enzyme-based carbonate precipitation can achieve swell reductions comparable to the present MICP system (swell pressure: 6.5 vs. 2.02 kPa). However, the present RHB-MICP approach offers the additional advantage of sustained in-situ calcite production through living bacterial activity and the pozzolanic contribution of RHB, whereas EICP is limited by the finite catalytic lifespan of the applied urease. Conversely, EICP avoids the need for bacterial cultivation and offers simpler application protocols, making the two approaches complementary technologies for different field conditions.

Table 11. Comparative analysis: RHB and MICP bio-stimulation vs. other stabilizers for expansive soil stabilization.

Ref.	Stabilizing Agent (Contents, Optimum Content in wt%)	UCS (MPa)	STS (MPa)	Soaked CBR (%)	Free Swell Strain (%)	Swell Pressure (kPa)	FSI (%)	Linear Shrinkage (%)
Present Study	Rice Husk Biochar (0–4, 2) + MICP Bio-stimulation (2-and 4-day, 4 day)	0.072–0.148	0.012–0.045	2.5–4.7	8.1–53.1	6.5–96.5	1.5–82.6	2.2–14.4
(Tiwari et al. 2021)	MICP Bio-stimulation (nutrient broth, 1–4 day mellowing)	0.068–0.225	0.024–0.325	×	1.4–10.25	41–210	15–120	×
Islam et al. (2020)	MICP Bio-stimulation (enrichment + cementation solution, TSDS)	0.15–0.40	×	×	3–52	25–99	×	×
Li et al. (2018a)	Fly Ash (0–50, 25) + Biocement (*B. megaterium*, 5%)	0.143–0.719	×	×	~2–7	×	×	×
Paul and Islam (2025)	MICP Bio-stimulation + Jute Fiber (0.25–1, 0.5)	0.137–0.209	0.072–0.124	4.3–4.6	8.4–24.5	9–39	×	4.3–14.1
Paul et al. (2025a)	SBA (2–12, 4) + Cement (5 and 7, 7)	0.96–2.36	0.14–0.75	42–51	1.24–21.31	1.5–14.9	2.73–27.27	×
Paul et al. (2025b)	Cement (5) + Jute Fiber (0.25–1, 0.5) + Nylon Fiber (0.25–1, 0.5)	1.16–2.36	0.35–0.98	28–31	7.87–39.35	5.71–59.02	×	1.83–6.24
Kumar et al. (2007)	FA (5–20) + Hydrated Lime (2–10) + Polyester Fiber (0.5–2)	0.32–0.65	0.04–0.10	×	×	×	×	×
Zha et al. (2008)	FA (3–15) + Hydrated Lime (0–3)	0.45–0.83	×	×	5.00–11.40	88–239	29–56	×
Liu et al. (2019)	Rice Husk Ash + Calcium Carbide Residue (0–20, 15)	0.95–2.60	×	×	6.12–26.50	100–425	×	×
Nezhad et al. (2021)	PET Fiber (0.5–2, 2) / Basalt Fiber (0.5–2, 2)	×	0.03–0.06	8.70–19.17	×	×	×	×
Dhorey et al. (2025a)	Red Mud (5–20, 10), GGBS (3–12, 12), FA (5–20, 20), SF (3–9, 9), Terrazyme + MICP (*Methylobacterium radiotolerans*)	0.169–0.509	×	×	×	×	×	×
Dhorey et al. (2025b)	Red Mud (5–20, 15) + MICP (*Methylobacterium radiotolerans*, 1 M urea, 1 M $CaCl_2$)	0.161–0.971	0.055–0.339	×	×	×	×	×
Dhorey et al. (2025c)	MICP (*Methylobacterium radiotolerans*, 0.1 M urea, 0.3 M $CaCl_2$, RSM optimized)	0.330–1.739	×	×	×	×	×	×
Mehmood et al. (2025)	EICP (Soybean Urease, 0.75 mol/L) + Eggshell Powder (0–18, 14)	0.17–0.50	×	1.7–16.1	×	10–250	×	×
Li et al. (2025)	SICP (Soybean Urease, 1 mol/L Equimolar Urea–$CaCl_2$)	0.18–0.27	×	×	×	121–168	×	2.6–8.3
Paul et al. (2026)	EICP (Urease, 20 g/L) + Sodium Alginate (0–1, 0.67)	0.072–0.232	0.008–0.051	×	4.11–53.07	2.02–96.47	4.5–100	5.33–14.43

Notes. RHB: Rice Husk Biochar; MICP: Microbially Induced Calcite Precipitation; SBA: Sugarcane Bagasse Ash; FA: Fly Ash; HL: Hydrated Lime; GGBS: Ground Granulated Blast-furnace Slag; SF: Silica Fume; RSM: Response Surface Methodology; TSDS: Treatment Solution Delivery System; EICP: Enzyme-Induced Carbonate Precipitation; SICP: Soybean-Induced Carbonate Precipitation; ESP: Eggshell Powder; ×: Not reported. UCS and STS ranges include both untreated and treated values where applicable. Optimum content shown in parentheses where reported.

3.8. Limitations and Practical Implications

Although the present study demonstrates the effectiveness of RHB-MICP biostimulation for stabilizing expansive subgrade soil under controlled laboratory conditions, several limitations should be noted. All experiments were performed on remolded specimens at laboratory scale, and the performance of the treatment under field conditions, where soil heterogeneity, groundwater fluctuations, stress variations, and seasonal climatic changes may influence behavior, remains to be verified. In addition, only one soil type, a fat clay (CH) collected from a single location, was investigated; therefore, the applicability of the optimum RHB content and mellowing period identified in this study to other expansive soils with different mineralogical and index properties requires further evaluation. The microbiological analysis was also limited, as 16S metagenomic sequencing was conducted on only three representative specimens (M0B0, M4B0, and M4B2). Moreover, dedicated long-term durability testing under repeated wetting-drying cycles was not performed. Nevertheless, the soaked CBR test and shrink-swell tests subjected the treated specimens to prolonged moisture exposure and thus provide indirect evidence of resistance to moisture-induced degradation.

Despite these limitations, the findings indicate strong practical potential. The optimum treatment condition, 2 % RHB with a 4-day mellowing period, produced the most pronounced improvement in strength and shrink-swell control. The increase in CBR is particularly important from a design perspective, as it can reduce the required subgrade thickness, thereby offering potential savings in construction materials and cost. The treated soil therefore shows promise for use as improved subgrade in low-volume flexible pavements, rural roads, embankment fills, and shallow foundations for lightly loaded structures on expansive soils. The proposed approach also offers important advantages over conventional stabilization methods. Biostimulation avoids the need for external bacterial cultivation and aseptic handling associated with bioaugmentation, making implementation simpler and potentially more economical. At the same time, rice husk is an abundant agricultural by-product and provides a low-cost feedstock for RHB production. This makes the method particularly relevant for rice-producing developing countries, where expansive soils and agricultural residues are both widely available. The approach also supports sustainable construction by valorizing waste biomass and reducing reliance on traditional chemical stabilizers such as lime and cement.

4. Conclusions

This study evaluated the effectiveness of combining MICP biostimulation with rice husk biochar (RHB) for stabilizing expansive subgrade soil. The results demonstrated that the integrated treatment significantly improved

the engineering behavior of the soil by reducing swell-related properties and enhancing strength characteristics. Compared with the untreated soil, the treated specimens showed marked reductions in free swell strain, swell pressure, free swell index, and linear shrinkage, together with clear improvements in UCS, STS, and CBR.

The treatment also promoted favorable chemical and microstructural changes in the soil matrix. Increased pH and calcite content confirmed the suitability of the bio-stimulation environment for carbonate precipitation. FTIR and SEM analyses further verified the formation of calcite and calcium silicate hydrate and revealed a denser, more compact soil structure with reduced voids and fissures. In addition, 16S metagenomic sequencing showed a microbial shift toward urease-positive groups, indicating that RHB enhanced the MICP biostimulation process.

The major contribution of this study is the demonstration that RHB can work synergistically with MICP biostimulation to improve both volume stability and strength of expansive soil, while also promoting favorable microbial and mineralogical transformations. These findings provide a promising basis for the development of more sustainable bio-mediated stabilization approaches for expansive subgrade soils. Future work should focus on field-scale validation, long-term durability, and performance under varying environmental conditions.

Declaration of interests

The authors declare no conflicts of interest, financial or personal, that could have influenced the work reported in this study.

Data availability

Data will be made available upon request.

Funding sources

This research was funded by RISE, BUET, under Grant ID: S2024-01-059.

References

Agustina, D.H., and Zainorabidin, A. (2020). “Evaluation of resilient modulus and unconfined compressive strength of subgrade.” *E3S Web of Conferences*, EDP Sciences.

Alhassan, M., and Mustapha, A.M. Effect of Rice Husk Ash on Cement Stabilized Laterite from Leonardo Electronic Journal of Practices and Technologies:

Anupam, A.K., Kumar, P., and Ransingchung, G.D. (2014). Performance evaluation of structural properties for soil stabilised using rice husk ash: *Road Materials and Pavement Design*, Vol. 15, No. 3, pp. 539–553, DOI: 10.1080/14680629.2014.891533.

ASTM C496/C496M − 17 (2011). Standard Test Method for Splitting Tensile Strength of Cylindrical Concrete Specimens ASTM C-496: *ASTM International*, No. March 1996, pp. 1–5.

ASTM D638. (2015). Standard Test Method for Tensile Properties. https://doi.org/10.1520/D0638-14.1

ASTM D1883 (2021). Standard Test Method for California Bearing Ratio (CBR) of Laboratory-Compacted Soils.:

ASTM D2487 (2013). Standard Practice for classification of Soils for Engineering purposes: *ASTM International*, Vol. 04, pp. 1–8, DOI: 10.1520/D2487-17E01.2.

ASTM D4373 (2021). Standard Test Method for Rapid Determination of Carbonate Content of Soils.

ASTM D4972 (2018). Standard Test Methods for pH of Soils.

ASTM D5102 (2009). Standard Test Methods for Unconfined Compressive Strength of Compacted Soil-Lime Mixtures: *ASTM International*, No. November, pp. 1–7, DOI: 10.1520/D5102-09.

Asuri, S., and Keshavamurthy, P. (2016). Expansive Soil Characterisation: an Appraisal: *INAE Letters*, Vol. 1, No. 1, pp. 29–33, DOI: 10.1007/s41403-016-0001-9.

Bailey, V.L., Fansler, S.J., Smith, J.L., and Bolton, H. (2011). Reconciling apparent variability in effects of biochar amendment on soil enzyme activities by assay optimization: *Soil Biology and Biochemistry*, Vol. 43, No. 2, pp. 296–301, DOI: 10.1016/J.SOILBIO.2010.10.014.

Barman, D., and Dash, S.K. (2022). Stabilization of expansive soils using chemical additives: A review: *Journal of Rock Mechanics and Geotechnical Engineering*, Vol. 14, No. 4, pp. 1319–1342, DOI: 10.1016/j.jrmge.2022.02.011.

Behzadipour, H., and Sadrekarimi, A. Biochar-assisted bio-cementation of a sand using native bacteria: DOI: 10.1007/s10064-021-02235-0/Published.

Bowles, J.E. (1992). Engineering properties of soils and their measurement: *Engineering properties of soils and their measurement.*, p. 241.

BS 1377 (1990). Methods of test for Soils for civil engineering purposes — Part 2: Classification tests.:

Bu, C., Wen, K., Liu, S., Ogbonnaya, U., and Li, L. (2018). Development of bio-cemented constructional materials through microbial induced calcite precipitation: *Materials and Structures/Materiaux et Constructions*, Vol. 51, No. 1, pp. 1–11, DOI: 10.1617/s11527-018-1157-4.

Buhler, R.L., and Cerato, A.B. (2007). "Stabilization of Oklahoma Expansive Soils using Lime and Class C Fly Ash." *Problematic Soils and Rocks and In Situ Characterization, GeoDenver,*, p. 1–10.

Cantrell, K.B., Hunt, P.G., Uchimiya, M., Novak, J.M., and Ro, K.S. (2012). Impact of pyrolysis temperature and manure source on physicochemical characteristics of biochar: *Bioresource Technology*, Vol. 107, pp. 419–428, DOI: 10.1016/J.BIORTECH.2011.11.084.

Chen, F.H. (1975). *Foundations on Expansive Soils.*, Elsevier Scientific Pub. Co.

Cheng, L., and Cord-Ruwisch, R. (2014). Upscaling Effects of Soil Improvement by Microbially Induced Calcite Precipitation by Surface Percolation: *Geomicrobiology Journal*, Vol. 31, No. 5, pp. 396–406, DOI: 10.1080/01490451.2013.836579.

Chittoori, and Neupane, S. (2019). *Evaluating the Application of Microbial Induced Calcite Precipitation Technique to Stabilize Expansive Soils*, Springer International Publishing.

Chittoori, Pathak, A., Burbank, M., and Islam, Md.T. (2020). Application of Bio-Stimulated Calcite Precipitation to Stabilize Expansive Soils: Field Trials: No. February, pp. 111–120, DOI: 10.1061/9780784482834.013.

Das, B.M. (2019). *Advanced Soil Mechanics*, CRC Press.

DeJong, J.T., Fritzges, M.B., and Nüsslein, K. (2006). Microbially Induced Cementation to Control Sand Response to Undrained Shear: *Journal of Geotechnical and Geoenvironmental Engineering*, Vol. 132, No. 11, pp. 1381–1392, DOI: 10.1061/(asce)1090-0241(2006)132:11(1381).

DeJong, J.T., Mortensen, B.M., Martinez, B.C., and Nelson, D.C. (2010). Bio-mediated soil improvement: *Ecological Engineering*, Vol. 36, No. 2, pp. 197–210, DOI: 10.1016/J.ECOLENG.2008.12.029.

Dejong, J.T., Soga, K., Kavazanjian, E., Burns, S., Van Paassen, L.A., AL Qabany, A., Aydilek, A., Bang, S.S., Burbank, M., Caslake, L.F., Chen, C.Y., Cheng, X., Chu, J., Ciurli, S., Esnault-Filet, A., et al. (2013). Biogeochemical processes and geotechnical applications: Progress, opportunities and challenges: *Geotechnique*, Vol. 63, No. 4, pp. 287–301, DOI: 10.1680/GEOT.SIP13.P.017.

Dhorey, A.R., Nikose, S., and Patel, A. (2026). Geotechnical Application of Methylobacterium radiotolerans in Expansive Soil: Bacterial Isolation and Optimization Using Response Surface Method : *Journal of Materials in Civil Engineering*, Vol. 38, No. 2, DOI: 10.1061/jmcee7.mteng-20252.

Dhorey, A.R., Nikose, S., and Patel, A. (2025a). Enhancing Geotechnical Properties of Red Mud Stabilized Black Cotton Soil with Microbially Induced Calcite Precipitation: A Comprehensive Performance and Microstructural Analysis: *Arabian Journal for Science and Engineering*, DOI: 10.1007/s13369-025-10273-z.

Dhorey, A.R., Nikose, S., and Patel, A. (2025b). "Performance Evaluation of Expansive Soil Treated with MICP and Industrial Waste Materials." *Proceedings of GeoMandu 2024*,, p. 353–363.

Djellali, A., Houam, A., and Saghafi, B. (2017). Indirect Estimation of Swelling Pressure of Clayey Subgrade Under Pavement Structures: *Arabian Journal for Science and Engineering*, Vol. 42, No. 9, pp. 3991–3999, DOI: 10.1007/S13369-017-2546-7/METRICS.

Douglas, S., and Beveridge, T.J. (2006). Mineral formation by bacteria in natural microbial communities: *FEMS Microbiology Ecology*, Vol. 26, No. 2, pp. 79–88, DOI: 10.1111/j.1574-6941.1998.tb00494.x.

Ekprasert, J., Fongkaew, I., Chainakun, P., Kamngam, R., and Boonsuan, W. (2020). Investigating mechanical properties and biocement application of CaCO3 precipitated by a newly-isolated Lysinibacillus sp. WH using artificial neural networks: *Scientific Reports 2020 10:1*, Vol. 10, No. 1, pp. 1–13, DOI: 10.1038/s41598-020-73217-7.

Garg, A., Huang, H., Kushvaha, V., Madhushri, P., Kamchoom, V., Wani, I., Koshy, N., Zhu, H.-H., Garg, A., Huang, H., Kushvaha, V., Madhushri, P., Kamchoom, V., Wani, I., Koshy, N., et al. (2019). Mechanism of biochar soil pore-gas-water interaction: gas properties of biochar-amended sandy soil at different degrees of compaction using KNN modeling: *AcGeo*, Vol. 68, No. 1, pp. 207–217, DOI: 10.1007/S11600-019-00387-Y.

Gaskin, J.W., Steiner, C., Harris, K., Das, K.C., and Bibens, B. (2008). Effect of Low-Temperature Pyrolysis Conditions on Biochar for Agricultural Use: *Transactions of the ASABE*, Vol. 51, No. 6, pp. 2061–2069, DOI: 10.13031/2013.25409.

Gat, D., Ronen, Z., and Tsesarsky, M. (2017). Long-term sustainability of microbial-induced CaCO3 precipitation in aqueous media: *Chemosphere*, Vol. 184, pp. 524–531, DOI: 10.1016/j.chemosphere.2017.06.015.

Ghanizadeh, A.R., Salehi, M., Mamou, A., Koutras, E.I., Jalali, F., and Asteris, P.G. (2024). Investigation of Subgrade Stabilization Life-Extending Benefits in Flexible Pavements Using a

Non-Linear Mechanistic-Empirical Analysis: *Infrastructures*, Vol. 9, No. 2, DOI: 10.3390/infrastructures9020033.

Gomez, M.G., Anderson, C.M., Graddy, C.M.R., DeJong, J.T., Nelson, D.C., and Ginn, T.R. (2017). Large-Scale Comparison of Bioaugmentation and Biostimulation Approaches for Biocementation of Sands: *Journal of Geotechnical and Geoenvironmental Engineering*, Vol. 143, No. 5, pp. 1–13, DOI: 10.1061/(asce)gt.1943-5606.0001640.

Gomez, M.G., Graddy, C.M.R., DeJong, J.T., Nelson, D.C., and Tsesarsky, M. (2018). Stimulation of Native Microorganisms for Biocementation in Samples Recovered from Field-Scale Treatment Depths: *Journal of Geotechnical and Geoenvironmental Engineering*, Vol. 144, No. 1, pp. 1–13, DOI: 10.1061/(asce)gt.1943-5606.0001804.

Graddy, C.M.R., Gomez, M.G., Kline, L.M., Morrill, S.R., Dejong, J.T., and Nelson, D.C. (2018). Diversity of Sporosarcina -like Bacterial Strains Obtained from Meter-Scale Augmented and Stimulated Biocementation Experiments: *Environmental Science and Technology*, Vol. 52, No. 7, pp. 3997–4005, DOI: 10.1021/ACS.EST.7B04271/SUPPL_FILE/ES7B04271_SI_001.PDF.

GuhaRay, A., Guoxiong, M., Sarkar, A., Bordoloi, S., Garg, A., and Pattanayak, S. (2019). Geotechnical and chemical characterization of expansive clayey soil amended by biochar derived from invasive weed species Prosopis juliflora: *Innovative Infrastructure Solutions*, Vol. 4, No. 1, DOI: 10.1007/s41062-019-0231-2.

Hammes, F., and Verstraete, W. (2002). Key roles of pH and calcium metabolism in microbial carbonate precipitation: *Reviews in Environmental Science and Biotechnology*, Vol. 1, No. 1, pp. 3–7, DOI: 10.1023/A:1015135629155/METRICS.

Holtz, W.G., and Gibbs, H.J. (1956). Engineering properties of expansive clays: *Transactions of the American Society of Civil Engineers*,.

Hossain, M.Z., Bahar, M.M., Sarkar, B., Donne, S.W., Ok, Y.S., Palansooriya, K.N., Kirkham, M.B., Chowdhury, S., and Bolan, N. (2020a). Biochar and its importance on nutrient dynamics in soil and plant: *Biochar*, Vol. 2, No. 4, pp. 379–420, DOI: 10.1007/S42773-020-00065-Z.

Hossain, N., Nizamuddin, S., Griffin, G., Selvakannan, P., Mubarak, N.M., and Mahlia, T.M.I. (2020b). Synthesis and characterization of rice husk biochar via hydrothermal carbonization for wastewater treatment and biofuel production: *Scientific Reports*, Vol. 10, No. 1, DOI: 10.1038/s41598-020-75936-3.

Hossain, M.K., Strezov Vladimir, V., Chan, K.Y., Ziolkowski, A., and Nelson, P.F. (2011). Influence of pyrolysis temperature on production and nutrient properties of wastewater sludge biochar: *Journal of Environmental Management*, Vol. 92, No. 1, pp. 223–228, DOI: 10.1016/J.JENVMAN.2010.09.008.

Hussain, R., and Ravi, K. (2022). Investigating biochar-amended soil as a potential lightweight material for embankments: *Ecological Engineering*, Vol. 180, DOI: 10.1016/j.ecoleng.2022.106645.

Ian Tiseo (2023). Global waste generation - statistics & facts | Statista: *Statista*,.

Ikeagwuani, C.C., and Nwonu, D.C. (2019). Emerging trends in expansive soil stabilisation: A review: *Journal of Rock Mechanics and Geotechnical Engineering*, Vol. 11, No. 2, pp. 423–440, DOI: 10.1016/j.jrmge.2018.08.013.

Ikechukwu, A.F., Hassan, M.M., and Moubarak, A. (2021). Swelling stress effects on shear strength resistance of subgrades: *International Journal of Geotechnical Engineering*, Vol. 15, No. 8, pp. 939–949, DOI: 10.1080/19386362.2019.1656445.

Inyang, M., and Dickenson, E. (2015). The potential role of biochar in the removal of organic and microbial contaminants from potable and reuse water: A review: *Chemosphere*, Vol. 134, pp. 232–240, DOI: 10.1016/j.chemosphere.2015.03.072.

IRC-37 (2012). Tentative guidelines for the design of flexible pavements.:

IS: 1498 (1970) (reaffirmed 1987) Indian standard classification and identification of soils for general engineering purposes.

IS 2720 (1991). Methods of test for soils Part 10: Determination of unconfined compressive strength: *BIS, New Delhi, India*.

Islam, Chittoori, B.C.S., and Burbank, M. (2020). "Evaluating the Applicability of Biostimulated Calcium Carbonate Precipitation to Stabilize Clayey Soils." *Journal of Materials in Civil Engineering*,.

Ito, M. (2013). Engineering properties of a vertisolic expansive soil deposit: *Engineering Geology*, Vol. 152, No. 1, pp. 10–16, DOI: 10.1016/j.enggeo.2012.10.004.

Ivanov, V., and Chu, J. (2008). Applications of microorganisms to geotechnical engineering for bioclogging and biocementation of soil in situ: *Reviews in Environmental Science and Biotechnology*, Vol. 7, No. 2, pp. 139–153, DOI: 10.1007/S11157-007-9126-3.

Jang, J., and Jia, P. (2020). A Review of the Application of Biopolymers on Geotechnical Engineering and the Strengthening Mechanisms between Typical Biopolymers and Soils: *Advances in Materials Science and Engineering*, Vol. 2020, DOI: 10.1155/2020/1465709.

Jindo, K., Mizumoto, H., Sawada, Y., Sanchez-Monedero, M.A., and Sonoki, T. (2014). Physical and chemical characterization of biochars derived from different agricultural residues: *Biogeosciences*, Vol. 11, No. 23, pp. 6613–6621, DOI: 10.5194/bg-11-6613-2014.

Jones, D.E., and Holtz, W.G. (1973). Expansive soils-the hidden disaster: *American Society of Civil Engineers*, Vol. 43, No. 8, pp. 49–51.

Kaleli, M.J., Kamweru, P.K., Gichumbi, J.M., and Ndiritu, F.G. (2020). Characterization of rice husk ash prepared by open air burning and furnace calcination: *Journal of Chemical Engineering and Materials Science*, Vol. 11, No. 2, pp. 24–30, DOI: 10.5897/jcems2020.0348.

Kavazanjian, E., and Karatas, I. (2008). "Microbiological improvement of the physical properties of soil." *International Conference on Case Histories in Geotechnical Engineering*,, p. 1–10.

Kloss, S., Zehetner, F., Dellantonio, A., Hamid, R., Ottner, F., Liedtke, V., Schwanninger, M., Gerzabek, M.H., and Soja, G. (2012). Characterization of Slow Pyrolysis Biochars: Effects of Feedstocks and Pyrolysis Temperature on Biochar Properties: *Journal of Environmental Quality*, Vol. 41, No. 4, pp. 990–1000, DOI: 10.2134/JEQ2011.0070.

Kong, S.H., Loh, S.K., Bachmann, R.T., Rahim, S.A., and Salimon, J. (2014). Biochar from oil palm biomass: A review of its potential and challenges: *Renewable and Sustainable Energy Reviews*, Vol. 39, pp. 729–739, DOI: 10.1016/J.RSER.2014.07.107.

Kumar, A., Walia, B.S., and Bajaj, A. (2007). Influence of Fly Ash, Lime, and Polyester Fibers on Compaction and Strength Properties of Expansive Soil: *Journal of Materials in Civil Engineering*, Vol. 19, No. 3, pp. 242–248, DOI: 10.1061/(asce)0899-1561(2007)19:3(242).

Li, M., Fang, C., Kawasaki, S., and Achal, V. (2018a). Fly ash incorporated with biocement to improve strength of expansive soil: *Scientific Reports*, Vol. 8, No. 1, pp. 4–10, DOI: 10.1038/s41598-018-20921-0.

Li, M., Fang, C., Kawasaki, S., and Achal, V. (2018b). Fly ash incorporated with biocement to improve strength of expansive soil: *Scientific Reports*, Vol. 8, No. 1, pp. 4–10, DOI: 10.1038/s41598-018-20921-0.

Li, T., Kong, L., and Guo, A. (2021). The deformation and microstructure characteristics of expansive soil under freeze–thaw cycles with loads: *Cold Regions Science and Technology*, Vol. 192, DOI: 10.1016/j.coldregions.2021.103393.

Li, M., Liu, W., Zhang, J., Lang, C., Xu, G., Zhu, L., and Tang, Q. (2025). Soybean-urease-induced CaCO3 precipitation as a new geotechnique for improving expansive soil: *Acta Geotechnica*, Vol. 20, No. 4, pp. 1877–1890, DOI: 10.1007/s11440-024-02481-y.

Liu, Y., Chang, C.W., Namdar, A., She, Y., Lin, C.H., Yuan, X., and Yang, Q. (2019). Stabilization of expansive soil using cementing material from rice husk ash and calcium carbide residue: *Construction and Building Materials*, Vol. 221, pp. 1–11, DOI: 10.1016/j.conbuildmat.2019.05.157.

Lu, S.G., Sun, F.F., and Zong, Y.T. (2014a). Effect of rice husk biochar and coal fly ash on some physical properties of expansive clayey soil (Vertisol): *Catena*, Vol. 114, pp. 37–44, DOI: 10.1016/J.CATENA.2013.10.014.

Lu, S.G., Sun, F.F., and Zong, Y.T. (2014b). Effect of rice husk biochar and coal fly ash on some physical properties of expansive clayey soil (Vertisol): *Catena*, Vol. 114, pp. 37–44, DOI: 10.1016/j.catena.2013.10.014.

Madadi, A., and Wei, J. (2022). Characterization of Calcium Silicate Hydrate Gels with Different Calcium to Silica Ratios and Polymer Modifications: *Gels*, Vol. 8, No. 2, DOI: 10.3390/gels8020075.

Mehmood, M., Guo, Y., Liu, Y., Wang, L., Nie, W., Uge, B.U., Ali, S., Xuanyu, C., and Zhao, Y. (2025). Experimental study on the engineering characteristics of expansive soil improved conjointly using enzyme induced carbonate precipitation and eggshell powder: *Soils and Foundations*, Vol. 65, No. 1, p. 101567, DOI: 10.1016/j.sandf.2025.101567.

Morales, L.F., Herrera, K., López, J.E., and Saldarriaga, J.F. (2021). Use of biochar from rice husk pyrolysis: assessment of reactivity in lime pastes: *Heliyon*, Vol. 7, No. 11, DOI: 10.1016/j.heliyon.2021.e08423.

Mostafa, A.E.A., Eisa, M., and Ibrahim, M.F. (2024). Effect of stabilizing subgrade layer using various additives on the flexible pavement design: *Innovative Infrastructure Solutions*, Vol. 9, No. 5, DOI: 10.1007/s41062-024-01430-8.

Nelson, J.D., and Miller, D.J. (1992). *Expansive soils : problems and practice in foundation and pavement engineering*, J. Wiley.

Nezhad, M.G., Tabarsa, A., and Latifi, N. (2021). Effect of natural and synthetic fibers reinforcement on California bearing ratio and tensile strength of clay: *Journal of Rock Mechanics and Geotechnical Engineering*, Vol. 13, No. 3, pp. 626–642, DOI: 10.1016/j.jrmge.2021.01.004.

Ng, C.W.W., Ni, J.J., and Leung, A.K. (2020). Effects of plant growth and spacing on soil hydrological changes: A field study: *Geotechnique*, Vol. 70, No. 10, pp. 867–881, DOI: 10.1680/JGEOT.18.P.207/ASSET/IMAGES/SMALL/JGEOT.18.P.207-F12.GIF.

Pan, Z., Garg, A., Huang, S., and Mei, G. (2021a). Swelling Suppression Mechanism of Compacted Expansive Soil Amended with Animal and Plant Based Biochar: *Waste and Biomass Valorization*, Vol. 12, No. 5, pp. 2653–2664, DOI: 10.1007/s12649-020-01172-5.

Pan, Z., Garg, A., Huang, S., and Mei, G. (2021b). Swelling Suppression Mechanism of Compacted Expansive Soil Amended with Animal and Plant Based Biochar: *Waste and Biomass Valorization*, Vol. 12, No. 5, pp. 2653–2664, DOI: 10.1007/s12649-020-01172-5.

Panda, D., Saini, C., Kumar, E.A., and Singh, S.K. (2020). In situ casting of rice husk ash in metal organic frameworks induces enhanced CO2 capture performance: *Scientific Reports*, Vol. 10, No. 1, pp. 1–12, DOI: 10.1038/s41598-020-77213-9.

Paul, S., Chakraborty, P., Anwar, A.B., Mortoza, G., and Sukti, L.S. (2025a). Effect of Cement and Sugarcane Bagasse Ash on the Micro-mechanical Characteristics of Expansive Soil: *Results in Engineering*, p. 106874, DOI: https://doi.org/10.1016/j.rineng.2025.106874.

Paul, S., Bin Faruque, A., Mottaqi, A., and Binta Anwar, A. (2026a). Enhancing Shear Strength of Sandy Soils Using Enzyme-Induced Carbonate Precipitation and Sodium Alginate Biopolymer: *Geo-Congress 2026*, pp. 375–384, DOI: 10.1061/9780784486764.037.

Paul, S., Bin Faruque, A., Mottaqi, A., and Islam Audri, O. (2026b). A Sustainable Hybrid Stabilization Approach for Expansive Soils: Integrating Enzyme-Induced Carbonate Precipitation with Sodium Alginate Biopolymer: *Geo-Congress 2026*, pp. 240–250, DOI: 10.1061/9780784486764.024.

Paul, S., Faruque, A. Bin, Mottaqi, A., and Audri, O.I. (2026c). "A Sustainable Hybrid Stabilization Approach for Expansive Soils: Integrating Enzyme-Induced Carbonate Precipitation with Sodium Alginate Biopolymer." *Geo-Congress 2026*,, p. 240–250.

Paul, S., and Islam, M.S. (2025). Sustainable stabilisation of expansive subgrade soil using bio-stimulation based microbially induced calcite precipitation process and waste fibre reinforcement: *Road Materials and Pavement Design*, Vol. 0, No. 0, pp. 1–49, DOI: 10.1080/14680629.2025.2505597.

Paul, S., Islam, M.S., and Chakma, N. (2024). Effectiveness of areca fiber and cement on the engineering characteristics of compressed stabilized earth blocks: *Construction and Building Materials*, Vol. 427, No. April, p. 136290, DOI: 10.1016/j.conbuildmat.2024.136290.

Paul, S., Islam, M.S., and Elahi, T.E. (2023). Potential of waste rice husk ash and cement in making compressed stabilized earth blocks: Strength, durability and life cycle assessment: *Journal of Building Engineering*, p. 106727, DOI: 10.1016/J.JOBE.2023.106727.

Paul, S., Tasnim, A., and Majumder, J. (2025b). Enhancement of Micro-mechanical Characteristics of Expansive Soil through Synergistic Incorporation of Jute and Nylon Fibers with Cement: *Results in Engineering*, Vol. 26, No. March, p. 104685, DOI: 10.1016/j.rineng.2025.104685.

Petry, T.M., and Little, D.N. (2003). Review of Stabilization of Clays and Expansive Soils in Pavements and Lightly Loaded Structures - History, Practice, and Future: *Perspectives in Civil Engineering: Commemorating the 150th Anniversary of the American Society of Civil Engineers*, Vol. 14, No. 6, pp. 307–320, DOI: 10.1061/(asce)0899-1561(2002)14:6(447).

Prendergast-Miller, M.T., Duvall, M., and Sohi, S.P. (2011). Localisation of nitrate in the rhizosphere of biochar-amended soils: *Soil Biology and Biochemistry*, Vol. 43, No. 11, pp. 2243–2246, DOI: 10.1016/J.SOILBIO.2011.07.019.

Puppala, A.J., and Pedarla, A. (2017). Innovative ground improvement techniques for expansive soils: *Innovative Infrastructure Solutions*, Vol. 2, No. 1, p. 24, DOI: 10.1007/s41062-017-0079-2.

Reddy, K.R., Yaghoubi, P., and Yukselen-Aksoy, Y. (2015). Effects of biochar amendment on geotechnical properties of landfill cover soil: *Waste management & research : the journal of the International Solid Wastes and Public Cleansing Association, ISWA*, Vol. 33, No. 6, pp. 524–532, DOI: 10.1177/0734242X15580192.

Ren, S., Lei, H., Wang, L., Bu, Q., Chen, S., and Wu, J. (2014). Hydrocarbon and hydrogen-rich syngas production by biomass catalytic pyrolysis and bio-oil upgrading over biochar catalysts: *RSC Advances*, Vol. 4, No. 21, pp. 10731–10737, DOI: 10.1039/C4RA00122B.

Road pavement design manual (1999). Government of the People's Republic of Bangladesh

Romdhane, L., Awad, Y.M., Radhouane, L., Dal Cortivo, C., Barion, G., Panozzo, A., and Vamerali, T. (2019). Wood biochar produces different rates of root growth and transpiration in two maize hybrids (Zea mays L.) under drought stress: *Archives of Agronomy and Soil Science*, Vol. 65, No. 6, pp. 846–866, DOI: 10.1080/03650340.2018.1532567.

Seed, H.B., Woodward, R.J., and Lundgren, R. (1962). Prediction of Swelling Potential for Compacted Clays: *Journal of the Soil Mechanics and Foundations Division*, Vol. 88, No. 3, pp. 53–87, DOI: 10.1061/jsfeaq.0000431.

Shekhawat, P., Sharma, G., and Singh, R.M. (2020). Potential Application of Heat Cured Eggshell Powder and Flyash-Based Geopolymer in Pavement Construction: *International Journal of Geosynthetics and Ground Engineering*, Vol. 6, No. 2, pp. 1–17, DOI: 10.1007/S40891-020-00213-2/FIGURES/17.

Sikder, T., Paul, S., Islam, M.S., and Paul, S. (2026). Utilisation of fly ash and sewage sludge ash based geopolymer with cement for the production of compressed stabilized earthen block compressed stabilized earthen block: *European Journal of Environmental and Civil Engineering*, Vol. 30, No. 1, p., DOI: 10.1080/19648189.2026.2618000.

Singh, B., Singh, B.P., and Cowie, A.L. (2010). Characterisation and evaluation of biochars for their application as a soil amendment: *Soil Research*, Vol. 48, No. 7, pp. 516–525, DOI: 10.1071/SR10058.

Singh, R., Srivastava, P., Singh, P., Sharma, A.K., Singh, H., and Raghubanshi, A.S. (2019). Impact of rice-husk ash on the soil biophysical and agronomic parameters of wheat crop under a dry tropical ecosystem: *Ecological Indicators*, Vol. 105, No. April, pp. 505–515, DOI: 10.1016/j.ecolind.2018.04.043.

Singh Yadav, S.P., Bhandari, S., Bhatta, D., Poudel, A., Bhattarai, S., Yadav, P., Ghimire, N., Paudel, P., Paudel, P., Shrestha, J., and Oli, B. (2023). Biochar application: A sustainable approach to improve soil health: *Journal of Agriculture and Food Research*, Vol. 11, DOI: 10.1016/j.jafr.2023.100498.

Su, H., Xiao, H., Li, Z., Tian, X., Luo, S., Yu, X., and Ouyang, Q. (2022). Experimental Study on Microstructure Evolution and Fractal Features of Expansive Soil Improved by MICP Method: *Frontiers in Materials*, Vol. 9, No. March, pp. 1–10, DOI: 10.3389/fmats.2022.842887.

Sun, F., and Lu, S. (2014). Biochars improve aggregate stability, water retention, and pore-space properties of clayey soil: *Journal of Plant Nutrition and Soil Science*, Vol. 177, No. 1, pp. 26–33, DOI: 10.1002/JPLN.201200639.

Tiwari, N., and Satyam, N. (2022). An experimental study on strength improvement of expansive subgrades by polypropylene fibers and geogrid reinforcement: *Scientific Reports*, Vol. 12, No. 1, pp. 1–9, DOI: 10.1038/s41598-022-10773-0.

Tiwari, N., Satyam, N., and Sharma, M. (2021). Micro-mechanical performance evaluation of expansive soil biotreated with indigenous bacteria using MICP method: *Scientific Reports*, Vol. 11, No. 1, pp. 1–12, DOI: 10.1038/s41598-021-89687-2.

Tsesarsky, M., Gat, D., and Ronen, Z. (2018). Biological aspects of microbial-induced calcite precipitation: *Environmental Geotechnics*, Vol. 5, No. 2, pp. 69–78, DOI: 10.1680/JENGE.15.00070.

Vijayan, D.S., and Parthiban, D. (2020). Effect of Solid waste based stabilizing material for strengthening of Expansive soil- A review: *Environmental Technology and Innovation*, Vol. 20, p. 101108, DOI: 10.1016/j.eti.2020.101108.

Villarreal, J., and Wang, F. (2021). Feasibility Study on Biochar-Treated Expansive Soils: *International Journal of Geosynthetics and Ground Engineering*, Vol. 7, No. 2, DOI: 10.1007/s40891-021-00277-8.

Wang, Y., Jiang, N., Saracho, A.C., Doygun, O., Du, Y., and Han, X. (2023). Compressibility characteristics of bio-cemented calcareous sand treated through the bio-stimulation approach: *Journal of Rock Mechanics and Geotechnical Engineering*, Vol. 15, No. 2, pp. 510–522, DOI: 10.1016/J.JRMGE.2022.05.007.

Wang, X., Zhou, W., Liang, G., Song, D., and Zhang, X. (2015). Characteristics of maize biochar with different pyrolysis temperatures and its effects on organic carbon, nitrogen and enzymatic

activities after addition to fluvo-aquic soil: *Science of The Total Environment*, Vol. 538, pp. 137–144, DOI: 10.1016/J.SCITOTENV.2015.08.026.

Wani, I., Kushvaha, V., Garg, A., Kumar, R., Naik, S., and Sharma, P. (2022). Review on effect of biochar on soil strength: Towards exploring usage of biochar in geo-engineering infrastructure: *Biomass Conversion and Biorefinery*, DOI: 10.1007/s13399-022-02795-5.

Xiao, P., Liu, H., Xiao, Y., Stuedlein, A.W., and Evans, T.M. (2018). Liquefaction resistance of bio-cemented calcareous sand: *Soil Dynamics and Earthquake Engineering*, Vol. 107, No. September 2017, pp. 9–19, DOI: 10.1016/j.soildyn.2018.01.008.

Xu, M., Ma, J., Zhang, X.H., Yang, G., Long, L.L., Chen, C., Song, C., Wu, J., Gao, P., and Guan, D.X. (2023). Biochar-bacteria partnership based on microbially induced calcite precipitation improves Cd immobilization and soil function: *Biochar*, Vol. 5, No. 1, DOI: 10.1007/s42773-023-00222-0.

Yan, P., Ma, Z., Li, H., Gong, P., Xu, M., and Chen, T. (2023). Laboratory tests, field application and carbon footprint assessment of cement-stabilized pure coal solid wastes as pavement base materials: *Construction and Building Materials*, Vol. 366, p. 130265, DOI: 10.1016/J.CONBUILDMAT.2022.130265.

Yu, X., Xiao, H., Li, Z., Qian, J., Luo, S., and Su, H. (2022). Experimental study on microstructure of unsaturated expansive soil improved by micp method: *Applied Sciences (Switzerland)*, Vol. 12, No. 1, DOI: 10.3390/app12010342.

Zada, U., Jamal, A., Iqbal, M., Eldin, S.M., Almoshaogeh, M., Bekkouche, S.R., and Almuaythir, S. (2023). Recent advances in expansive soil stabilization using admixtures: current challenges and opportunities: *Case Studies in Construction Materials*, Vol. 18, No. November 2022, p. e01985, DOI: 10.1016/j.cscm.2023.e01985.

Zha, F., Liu, S., Du, Y., and Cui, K. (2008). Behavior of expansive soils stabilized with fly ash: *Natural Hazards*, Vol. 47, No. 3, pp. 509–523, DOI: 10.1007/s11069-008-9236-4.

Zhao, Y., Fan, C., Ge, F., Cheng, X., and Liu, P. (2020). Enhancing Strength of MICP-Treated Sand with Scrap of Activated Carbon-Fiber Felt: *Journal of Materials in Civil Engineering*, Vol. 32, No. 4, p. 04020061, DOI: 10.1061/(ASCE)MT.1943-5533.0003136.

Zong, Y., Chen, D., and Lu, S. (2014). Impact of biochars on swell–shrinkage behavior, mechanical strength, and surface cracking of clayey soil: *Journal of Plant Nutrition and Soil Science*, Vol. 177, No. 6, pp. 920–926, DOI: 10.1002/JPLN.201300596.

Graphical Abstract

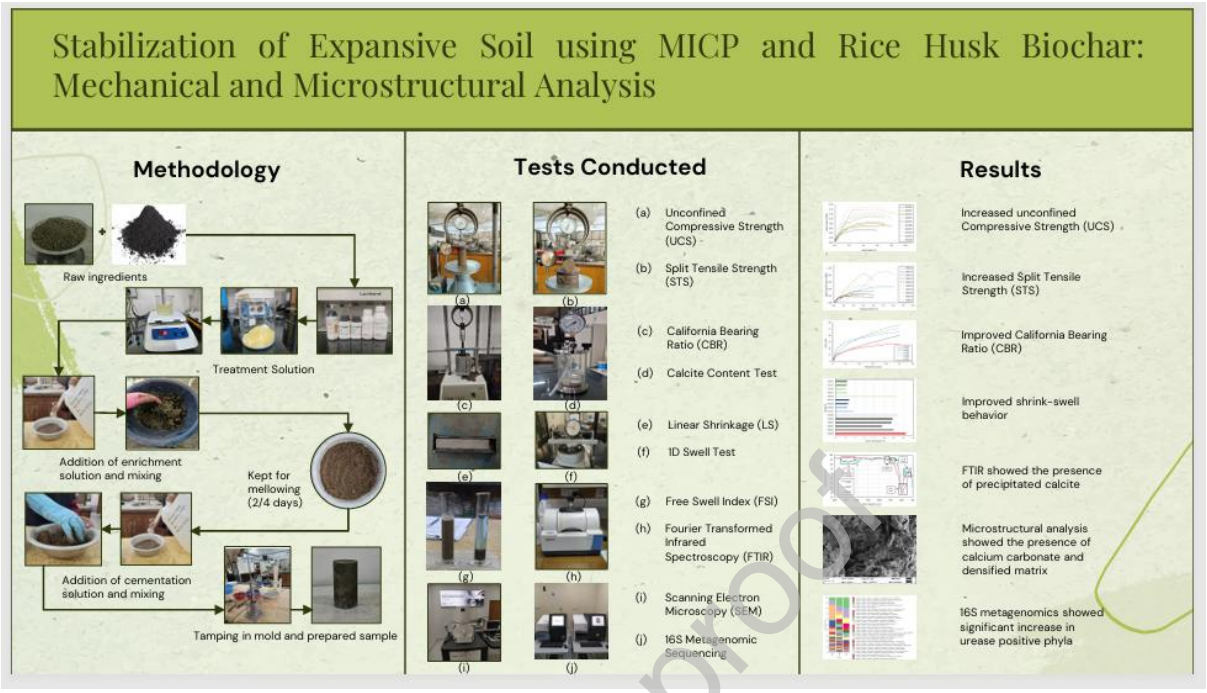

Declaration of interests

☒ The authors declare that they have no known competing financial interests or personal relationships that could have appeared to influence the work reported in this paper.

☐ The authors declare the following financial interests/personal relationships which may be considered as potential competing interests: